Full-Duplex FAS-assisted Base Station for ISAC

Boyi Tang, *Student Member, IEEE*, Hao Xu, *Senior Member, IEEE*,
Kai-Kit Wong, *Fellow, IEEE*, Kaitao Meng, *Member, IEEE*, Ross Murch, *Fellow, IEEE*,
Chan-Byoung Chae, *Fellow, IEEE*, and Yangyang Zhang

***Abstract*—This paper studies the use of multiple planar fluid antennas at a full-duplex base station (BS) for integrated sensing and communication (ISAC). In this model, the BS communicates with a downlink user, an uplink user, and performs target sensing simultaneously. Our objective is to maximize the communication sum-rate of the up and downlink users while meeting the sensing and power constraints. Given the problem is non-convex, we first reformulate the problem using the fractional programming (FP) framework. After that, we iteratively optimize the beamforming vectors of the BS, the uplink transmit power from the user, and the antenna positions of both transmit and receive fluid antenna systems (FASs) at the BS. In particular, the transmit and receive beamforming vectors are optimized by utilizing the majorization-minimization (MM) framework, and a closed-form solution for the uplink transmit power is derived. To optimize the BS antenna positions, we transform the problems into convex quadratically constrained quadratic programs (QCQP) by using Taylor series expansion. The subproblems can then be solved based on the successive convex approximation (SCA). Simulation results show that FAS can greatly improve the communication rate compared to the traditional fixed-position antenna (FPA) system.**

***Index Terms*—Fractional programming, fluid antenna system, full-duplex system, integrated sensing and communication.**

I. Introduction

THE SIXTH generation (6G) wireless network is hopeful to revolutionize communications to yet again an unprecedented level far beyond the current systems. This time there is huge excitement around artificial intelligence (AI) and sensing capabilities to innovate a plethora of applications [1], [2], [3]. The primary objectives in 6G can boil down to hitting data rates of 1 terabit per second (Tbps), achieving an extraordinary spectral efficiency of 1000 bps/Hz, and keeping latency as low as 1 microsecond (μs), according to [4].

To support massive connectivity, conventional schemes rely on multiuser multiple-input multiple-output (MIMO) antenna technologies [5]. Multiuser MIMO emerged as early as 2000 [6], [7] and classical results were reported in [8], [9]. Since the fourth generation (4G), multiuser MIMO has been the root of the physical layer in wireless communications. In recent years, multiuser MIMO has also evolved into massive MIMO, as a key attempt to simplify the precoding design [10], [11]. Extra-large MIMO (XL-MIMO) is also being regarded as one key direction to pursue in the 6G development [12].

While the push to include more antennas at the base station (BS) will continue, this is met with concern for the low power efficiency and the hefty cost of the increasing number of radio-frequency (RF) chains. This has motivated researchers to seek alternatives to enhance MIMO without necessarily increasing the number of antennas. One direction is to leverage the new generation of reconfigurable antennas that offers new degrees-of-freedom (DoFs) within the antenna itself to strengthen the physical layer. In 2020, Wong *et al.* presented a broad concept, referred to as fluid antenna system (FAS), for embracing all forms of shape and position reconfigurability in antennas for improving wireless communications [13], [14], [15]. A recent article in [16] provides a comprehensive tutorial on the topic whereas [17] gives theoretical foundation and interpretation to FAS from the electromagnetic perspective.

The concept of FAS is motivated by the advances in highly reconfigurable antenna structures such as liquid antennas [18], [19], movable arrays [20], [21], metamaterial based antennas [22], [23], [24] and reconfigurable pixels [25], [26], etc. The latter two technologies are particularly suitable since they have practically zero response time and the reconfigurability does not impose high power consumption like the first two.

Following the early results in [13], [14], [15], great efforts have been made to advance the research field. For example, [27] examined the use of FAS to enhance the performance in the millimeter-wave band while [28], [29], [30], [31] studied the performance of FAS under different channel models. FAS with continuous antenna positioning was investigated in [32]. More recently, FAS has also been employed at both ends of a communication channel, with its diversity and multiplexing tradeoff characterized in [33]. FAS has also been shown to be effective in raising the DoF for MIMO in multiuser channels [34] while [35] adopted FAS at the BSs in a cell-free setup.

A branch of research efforts also sees FAS applied to tackle a niche multiple access problem, the one that is able to serve many users on the same physical channel without the channel state information (CSI) at the transmitter side. This has led to the fluid antenna multiple access (FAMA) technique in [36]. Since then, a practical scheme, called slow FAMA [37], [38], was proposed to allow several users to share the same channel without precoding or interference cancellation. More research on FAMA can be found in [39], [40], [41], [42].

Additionally, the application of FAS has also extended to wireless powered communication systems [43], [44], physical-

The work of K. K. Wong is supported by the Engineering and Physical Sciences Research Council (EPSRC) under grant EP/W026813/1.

The work of R. Murch was supported by the Hong Kong Research Grants Council Area of Excellence Grant AoE/E-601/22-R.

The work of C. B. Chae is supported by the Institute for Information and Communication Technology Planning and Evaluation (IITP)/NRF grant funded by the Ministry of Science and ICT (MSIT), South Korea, under Grant RS-2024-00428780 and 2022R1A5A1027646.

B. Tang, K. Wong and K. Meng are with the Department of Electronic and Electrical Engineering, University College London, London WC1E7JE, United Kingdom. K. Wong is also affiliated with Yonsei Frontier Laboratory, Yonsei University, Seoul, 03722, Korea.

H. Xu is with the Frontiers Science Center for Mobile Information Communication and Security, Southeast University, Nanjing, China.

R. Murch is with the Department of Electronic and Computer Engineering and Institute for Advanced Study (IAS), Hong Kong University of Science and Technology, Clear Water Bay, Hong Kong SAR, China.

C. B. Chae is with School of Integrated Technology, Yonsei University, Seoul, 03722, Korea.

Y. Zhang is with Kuang-Chi Science Limited, Hong Kong SAR, China.

Corresponding author: Kai-Kit Wong (e-mail: kai-kit.wong@ucl.ac.uk).

layer security [45], [46] and near-field communications [47]. Needless to say, CSI is essential for a FAS-equipped terminal to optimize its antenna positioning. Several methods have been developed to tackle the channel estimation problems in FAS, including the successive Bayesian reconstructor [48], the low-sample-size sparse channel reconstruction (L3SCR) [49], and the linear minimum mean-squared error (LMMSE) technique [50]. In [51], the role of oversampling in the spatial domain in channel estimation for FAS channels was analyzed.

On the other hand, integrated sensing and communication (ISAC) in recent years has been a key driver for 6G [52]. The enormous interest in ISAC stems from the idea of combining sensing and communications into a unified system with shared resources [53], [54]. Despite its brilliance, ISAC puts pressure on the resources that are already very limited. Recent efforts therefore have explored the use of FAS to make ISAC viable. For example, [55] adopted a deep reinforcement learning based approach to maximize the sum rate in the downlink under a sensing constraint for a FAS-aided multiuser MIMO system. In [56] and [57], the results showed a considerable expansion of the ISAC tradeoff region when utilizing FAS compared to the fixed-position antenna (FPA) counterpart. The authors of [58], [59] further applied position-flexible antennas at both the transmitter and receiver sides to perform ISAC tasks in a bistatic radar system, where the transmitter and receiver are separated without self-interference (SI). Most recently, ISAC was also combined with backscatter communications in a FAS-aided system in [60], where the outage probability and ergodic sensing rate were derived. Recognizing the potential of smart environment technologies including FAS, [61] discusses the vision of future ISAC and its many opportunities.

On the other hand, there has been great interest to use full-duplex communication. Compared to traditional half-duplex systems that switch between transmission and reception, full-duplex communication significantly improves spectrum efficiency and reduces latency by enabling simultaneous transmission and reception over the same frequency band [62]. A stochastic-geometry-based analytical framework for the FAS-aided full-duplex communication was proposed in [63], while [64] presented a self-interference cancellation (SIC) framework for the FAS-aided full-duplex system. In [65], the authors investigated the outage probability of a multi-user full-duplex NOMA network, where the users were equipped with FAS. It is anticipated that in ISAC systems, full-duplex technology can further enhance sensing accuracy and real-time performance if the SI can be handled satisfactorily while reducing hardware overhead through the integrated architecture [66].

In this paper, we aim to further the efforts of using FAS for ISAC but different from previous studies, a full-duplex FAS-equipped BS is considered, meaning that the BS is required to transmit to a downlink user and also receive from an uplink user on the same physical data channel for higher spectral efficiency. Note that we consider the use of a mono-static radar and the SI in this paper to see if FAS has sufficient capability for the BS to mitigate the SI for full-duplex communication while performing the ISAC task. In particular, the BS has two separate, planar fluid antenna arrays, one for transmission and another for reception. Our objective is to jointly optimize

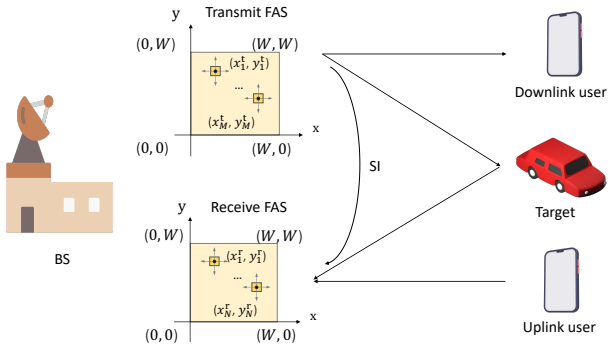

Fig. 1. An ISAC system with a full-duplex FAS-assisted BS, a downlink user, an uplink user, and a sensing target.

the beamforming vectors, the uplink transmit power, and the transmit and receive antenna positions of FAS at the BS to maximize the sum of the communication rates of the uplink and downlink users while satisfying the constraint of sensing signal-to-interference plus noise ratio (SINR).

Our main contributions are summarized as follows:

- First, we formulate the communication rate maximization problem for the full-duplex ISAC system, which is non-convex and intractable due to the coupled variables. To tackle this, we transform the problem using the fractional programming (FP) framework, and propose an alternative optimization algorithm to iteratively optimize the transmit and receive beamforming vectors, the transmit power of the uplink user, and both the transmit and receive antenna positions of the FAS at the BS. We obtain the transmit and receive beamforming vectors using majorization minimization (MM) and provide a closed-form solution for the uplink transmit power optimization.
- When the other variables are fixed, the subproblems of optimizing the transmit and receive antenna positions of the BS remain non-convex and hard to solve. To tackle this, we adopt Taylor series expansion to transform the problems into convex quadratically constrained quadratic program (QCQP) forms that can be solved efficiently. The antenna positions can then be optimized by the successive convex approximation (SCA) technique. Specifically, the proposed theorems and lemmas can reformulate the antenna position optimization problems that share the same structures in Table I into convex forms.
- Simulation results illustrate that using the proposed algorithm, the communication rate obtained by using FAS is much higher than that of the traditional FPA system. While the joint optimization of both transmit and receive antenna positions achieves a higher communication rate, updating only the transmit or receive FAS also greatly improves the system performance.

II. System Model

A. Signal Model

As shown in Fig. 1, we consider a FAS-assisted full-duplex ISAC system where the BS serves a downlink user, an uplink user, and attempts to sense a target simultaneously. Both users are equipped with a FPA. The BS has an M-antenna planar

TABLE I
SUMMARY OF THE PROPOSED THEOREMS AND LEMMAS

Theorem	Original Function Form	Surrogate Type	Surrogate Function Form	Parameters	Reference Equations
Theorem 1	$\lvert\boldsymbol{a}^T\boldsymbol{T}^H_{\chi 1}(\boldsymbol{V})\boldsymbol{b}\rvert^2$	Concave	$\boldsymbol{v}^T\hat{\boldsymbol{\Lambda}}\boldsymbol{v}+\hat{\boldsymbol{c}}\boldsymbol{v}+\hat{d}$	$\hat{\boldsymbol{\Lambda}}$ (NSD), $\hat{\boldsymbol{c}}$, $\hat{d}$	(53)
Theorem 1	$\lvert\boldsymbol{a}^T\boldsymbol{T}^H_{\chi 1}(\boldsymbol{V})\boldsymbol{b}\rvert^2$	Convex	$-\boldsymbol{v}^T\bar{\boldsymbol{\Lambda}}\boldsymbol{v}+\bar{\boldsymbol{c}}\boldsymbol{v}+\bar{d}$	$\bar{\boldsymbol{\Lambda}}$ (NSD), $\bar{\boldsymbol{c}}$, $\bar{d}$	(53), (56)
Theorem 2	$\mathrm{Re}\{\boldsymbol{a}^T\boldsymbol{T}^H_{\chi 1}(\boldsymbol{V})\boldsymbol{b}\}$	Concave	$\boldsymbol{v}^T\tilde{\boldsymbol{\Lambda}}\boldsymbol{v}+\tilde{\boldsymbol{c}}\boldsymbol{v}+\tilde{d}$	$\tilde{\boldsymbol{\Lambda}}$ (NSD), $\tilde{\boldsymbol{c}}$, $\tilde{d}$	(59)
Theorem 3	$\mathrm{Re}\{(\boldsymbol{a}^T\boldsymbol{T}^H_{\chi}(\boldsymbol{V})\boldsymbol{b})(\check{\boldsymbol{a}}^T\boldsymbol{T}^H_{\check{\chi}}(\boldsymbol{V})\boldsymbol{b})^H\}$	Convex	$\boldsymbol{v}^T\check{\boldsymbol{\Lambda}}\boldsymbol{v}+\check{\boldsymbol{c}}\boldsymbol{v}+\check{d}$	$\check{\boldsymbol{\Lambda}}$ (PSD), $\check{\boldsymbol{c}}$, $\check{d}$	(63)
Lemma 1	$\lvert\boldsymbol{b}^T\boldsymbol{R}_{\chi_2}(\boldsymbol{U})\boldsymbol{a}\rvert^2$	Concave	$\boldsymbol{u}^T\hat{\boldsymbol{\Omega}}\boldsymbol{u}+\hat{\boldsymbol{p}}\boldsymbol{u}+\hat{q}$	$\hat{\boldsymbol{\Omega}}$ (NSD), $\hat{\boldsymbol{p}}$, $\hat{q}$	(40) (53)
Lemma 1	$\lvert\boldsymbol{b}^T\boldsymbol{R}_{\chi_2}(\boldsymbol{U})\boldsymbol{a}\rvert^2$	Convex	$-\boldsymbol{u}^T\bar{\boldsymbol{\Omega}}\boldsymbol{u}+\bar{\boldsymbol{p}}\boldsymbol{u}+\bar{q}$	$\bar{\boldsymbol{\Omega}}$ (NSD), $\bar{\boldsymbol{p}}$, $\bar{q}$	(40) (53), (56)
Lemma 2	$\mathrm{Re}\{\boldsymbol{b}^T\boldsymbol{R}_{\chi_2}(\boldsymbol{U})\boldsymbol{a}\}$	Concave	$\boldsymbol{u}^T\tilde{\boldsymbol{\Omega}}\boldsymbol{u}+\tilde{\boldsymbol{p}}\boldsymbol{u}+\tilde{q}$	$\tilde{\boldsymbol{\Omega}}$ (NSD), $\tilde{\boldsymbol{p}}$, $\tilde{q}$	(66)
Lemma 3	$\mathrm{Re}\{(\boldsymbol{b}^T\boldsymbol{R}_{\check{\chi}}(\boldsymbol{U})\check{\boldsymbol{a}})(\boldsymbol{b}^T\boldsymbol{R}_{\chi}(\boldsymbol{U})\boldsymbol{a})^H\}$	Convex	$\boldsymbol{u}^T\check{\boldsymbol{\Omega}}\boldsymbol{u}+\check{\boldsymbol{p}}\boldsymbol{u}+\check{q}$	$\check{\boldsymbol{\Omega}}$ (PSD), $\check{\boldsymbol{p}}$, $\check{q}$	(46) (63)

FAS for transmiting signal and an N-antenna planar FAS for receiving signal. The size of each FAS is $\mathcal{S}=[0,W]\times[0,W]$. Each antenna at the FAS can be freely switched to any position within the given region instantly. The positions of the m-th transmit antenna and the n-th receive antenna are denoted by $\boldsymbol{v}_m=[x^{\mathrm{t}}_m,y^{\mathrm{t}}_m]^T$ and $\boldsymbol{u}_n=[x^{\mathrm{r}}_n,y^{\mathrm{r}}_n]^T$, respectively.

Let $\boldsymbol{w}_{\mathrm{t}}\in\mathbb{C}^{M\times 1}$and $s_{\mathrm{d}}\sim\mathcal{CN}(0,1)$ be the precoding vector and information symbol for the downlink user, respectively. Then the signal received by the donwlink user is given by

$$y_{\mathrm{d}}=\boldsymbol{h}_{\mathrm{d}}(\boldsymbol{V})\boldsymbol{w}_{\mathrm{t}}s_{\mathrm{d}}+n_{\mathrm{d}}, \tag{1}$$

where $\boldsymbol{h}_{\mathrm{d}}(\boldsymbol{V})\in\mathbb{C}^{1\times M}$ is the channel vector from the BS to the downlink user, $\boldsymbol{V}=[\boldsymbol{v}_1,\ldots,\boldsymbol{v}_M]\in\mathbb{R}^{2\times M}$, and $n_{\mathrm{d}}\sim\mathcal{CN}(0,\sigma^2_{\mathrm{d}})$ is the additive complex white Gaussian noise.

Similarly, denote the uplink symbol and channel by $s_{\mathrm{u}}\sim\mathcal{CN}(0,1)$ and $\boldsymbol{h}_{\mathrm{u}}(\boldsymbol{U})\in\mathbb{C}^{N\times 1}$, and $\boldsymbol{U}=[\boldsymbol{u}_1,\ldots,\boldsymbol{u}_N]\in\mathbb{R}^{2\times N}$. The received signal at the BS is written as

$$\boldsymbol{y}_{\mathrm{r}}=\boldsymbol{h}_{\mathrm{u}}(\boldsymbol{U})\sqrt{p_{\mathrm{u}}}s_{\mathrm{u}}+(\boldsymbol{H}_{\mathrm{s}}(\boldsymbol{V},\boldsymbol{U})+\boldsymbol{H}_{\mathrm{SI}}(\boldsymbol{V},\boldsymbol{U}))\,\boldsymbol{w}_{\mathrm{t}}s_{\mathrm{d}}+\boldsymbol{n}_{\mathrm{r}}, \tag{2}$$

where p_{u} is the transmit power of the uplink user, $\boldsymbol{H}_{\mathrm{s}}\in\mathbb{C}^{N\times M}$ and $\boldsymbol{H}_{\mathrm{SI}}\in\mathbb{C}^{N\times M}$ are the sensing and SI channels, respectively, and $\boldsymbol{n}_{\mathrm{r}}\sim\mathcal{CN}(\boldsymbol{0},\sigma^2_{\mathrm{r}}\boldsymbol{I})$ is the additive noise.

B. Channel Model

Here, we provide the expressions for the channel vectors $\boldsymbol{h}_{\mathrm{d}}$ and $\boldsymbol{h}_{\mathrm{u}}$, and the channel matrices $\boldsymbol{H}_{\mathrm{s}}$ and $\boldsymbol{H}_{\mathrm{SI}}$. Denote the azimuth and elevation angles of departure (AoDs) of the l-th downlink path by ϕ^{d}_l and θ^{d}_l, respectively. The propagation distance difference in the l-th path of the downlink channel between the position of the m-th transmit antenna $\boldsymbol{v}_m=[x^{\mathrm{t}}_m,y^{\mathrm{t}}_m]^T$ and its origin $[0,0]^T$ is

$$\rho^{\mathrm{d}}_l(\boldsymbol{v}_m)=x^{\mathrm{t}}_m\delta^{\mathrm{d}}_l+y^{\mathrm{t}}_m\xi^{\mathrm{d}}_l, \tag{3}$$

where $\delta^{\mathrm{d}}_l=\sin\theta^{\mathrm{d}}_l\cos\phi^{\mathrm{d}}_l$ and $\xi^{\mathrm{d}}_l=\cos\theta^{\mathrm{d}}_l$. The steering vector of the l-th path of the downlink channel is thus given by

$$\boldsymbol{t}^{\mathrm{d}}_l(\boldsymbol{V})=\left[e^{-j\frac{2\pi}{\lambda}\rho^{\mathrm{d}}_l(\boldsymbol{v}_1)},\ldots,e^{-j\frac{2\pi}{\lambda}\rho^{\mathrm{d}}_l(\boldsymbol{v}_M)}\right]^T\in\mathbb{C}^{M\times 1}, \tag{4}$$

where λ is the wavelength. Let L_{d} be the number of downlink propagation paths. Then we have

$$\boldsymbol{h}_{\mathrm{d}}(\boldsymbol{V})=\boldsymbol{1}^H\boldsymbol{\Gamma}_{\mathrm{d}}\boldsymbol{T}^H_{\mathrm{d}}(\boldsymbol{V})\in\mathbb{C}^{1\times M}, \tag{5}$$

in which $\boldsymbol{1}$ represents an all-ones column vector, $\boldsymbol{\Gamma}_{\mathrm{d}}=\mathrm{diag}\{\gamma^1_{\mathrm{d}},\ldots,\gamma^{L_{\mathrm{d}}}_{\mathrm{d}}\}\in\mathbb{C}^{L_{\mathrm{d}}\times L_{\mathrm{d}}}$ is the channel coefficient matrix, and $\boldsymbol{T}_{\mathrm{d}}(\boldsymbol{V})=\left[\boldsymbol{t}^{\mathrm{d}}_1(\boldsymbol{V}),\ldots,\boldsymbol{t}^{\mathrm{d}}_{L_{\mathrm{d}}}(\boldsymbol{V})\right]\in\mathbb{C}^{M\times L_{\mathrm{d}}}$.

Next, we denote the azimuth and elevation angles of arrival (AoAs) of the l-th uplink path by ϕ^{u}_l and θ^{u}_l, respectively. The propagation distance difference in the l-th path of the uplink channel between the n-th receive antenna position $\boldsymbol{u}_n=[x^{\mathrm{r}}_n,y^{\mathrm{r}}_n]^T$ and the origin is given by

$$\rho^{\mathrm{u}}_l(\boldsymbol{u}_n)=x^{\mathrm{r}}_n\delta^{\mathrm{u}}_l+y^{\mathrm{r}}_n\xi^{\mathrm{u}}_l, \tag{6}$$

where $\delta^{\mathrm{u}}_l=\sin\theta^{\mathrm{u}}_l\cos\phi^{\mathrm{u}}_l$ and $\xi^{\mathrm{u}}_l=\cos\theta^{\mathrm{u}}_l$. Then the steering vector of the uplink channel can be expressed as

$$\boldsymbol{r}^{\mathrm{u}}_l(\boldsymbol{U})=\left[e^{-j\frac{2\pi}{\lambda}\rho^{\mathrm{u}}_l(\boldsymbol{u}_1)},\ldots,e^{-j\frac{2\pi}{\lambda}\rho^{\mathrm{u}}_l(\boldsymbol{u}_N)}\right]^T\in\mathbb{C}^{N\times 1}. \tag{7}$$

Let L_{u} represent the number of uplink propagation paths. The uplink channel can then be written as

$$\boldsymbol{h}_{\mathrm{u}}(\boldsymbol{U})=\boldsymbol{R}_{\mathrm{u}}(\boldsymbol{U})\boldsymbol{\Gamma}_{\mathrm{u}}\boldsymbol{1}\in\mathbb{C}^{N\times 1}, \tag{8}$$

where $\boldsymbol{\Gamma}_{\mathrm{u}}=\mathrm{diag}\{\gamma^1_{\mathrm{u}},\ldots,\gamma^{L_{\mathrm{u}}}_{\mathrm{u}}\}\in\mathbb{C}^{L_{\mathrm{u}}\times L_{\mathrm{u}}}$ is the channel coefficient matrix and $\boldsymbol{R}_{\mathrm{u}}(\boldsymbol{U})=\left[\boldsymbol{r}^{\mathrm{u}}_1(\boldsymbol{U}),\ldots,\boldsymbol{r}^{\mathrm{u}}_{L_{\mathrm{u}}}(\boldsymbol{U})\right]\in\mathbb{C}^{N\times L_{\mathrm{u}}}$.

Consider a mono-static radar, and that the AoA and AoD of the sensing channel are the same. Denote the azimuth and elevation angles of the sensing path with respect to the BS by ϕ^{s} and θ^{s}, respectively. The receiving and transmitting steering vectors of the sensing channel are written as

$$\begin{cases}\boldsymbol{a}_{\mathrm{r}}(\boldsymbol{U})=\left[e^{-j\frac{2\pi}{\lambda}\rho_{\mathrm{r}}(\boldsymbol{u}_1)},\ldots,e^{-j\frac{2\pi}{\lambda}\rho_{\mathrm{r}}(\boldsymbol{u}_N)}\right]^T\in\mathbb{C}^{N\times 1},\\ \boldsymbol{a}_{\mathrm{t}}(\boldsymbol{V})=\left[e^{-j\frac{2\pi}{\lambda}\rho_{\mathrm{t}}(\boldsymbol{v}_1)},\ldots,e^{-j\frac{2\pi}{\lambda}\rho_{\mathrm{t}}(\boldsymbol{v}_M)}\right]^T\in\mathbb{C}^{M\times 1},\end{cases} \tag{9}$$

where $\rho_{\mathrm{r}}(\boldsymbol{u}_n)\triangleq x^{\mathrm{r}}_n\delta^{\mathrm{s}}+y^{\mathrm{r}}_n\xi^{\mathrm{s}}$ and $\rho_{\mathrm{t}}(\boldsymbol{v}_m)=x^{\mathrm{t}}_m\delta^{\mathrm{s}}+y^{\mathrm{t}}_m\xi^{\mathrm{s}}$ with $\delta^{\mathrm{s}}=\sin\theta^{\mathrm{s}}\cos\phi^{\mathrm{s}}$ and $\xi^{\mathrm{s}}=\cos\theta^{\mathrm{s}}$. The sensing channel can therefore be expressed as

$$\boldsymbol{H}_{\mathrm{s}}(\boldsymbol{V},\boldsymbol{U})=\alpha_{\mathrm{s}}\boldsymbol{a}_{\mathrm{r}}(\boldsymbol{U})\boldsymbol{a}^H_{\mathrm{t}}(\boldsymbol{V})\in\mathbb{C}^{N\times M}, \tag{10}$$

where α_{s} is the reflection coefficient including the path loss and the radar cross section (RCS).

Denote the AoDs and AoAs of the SI channel by $(\phi^{\mathrm{SI}}_{\mathrm{t},l},\theta^{\mathrm{SI}}_{\mathrm{t},l})$ and $(\phi^{\mathrm{SI}}_{\mathrm{r},l},\theta^{\mathrm{SI}}_{\mathrm{r},l})$, respectively. The receiving and transmiting steering vectors of the SI channel are found as

$$\begin{cases}\boldsymbol{r}^{\mathrm{SI}}_l(\boldsymbol{U})=\left[e^{-j\frac{2\pi}{\lambda}\rho^{\mathrm{SI}}_{\mathrm{r},l}(\boldsymbol{u}_1)},\ldots,e^{-j\frac{2\pi}{\lambda}\rho^{\mathrm{SI}}_{\mathrm{r},l}(\boldsymbol{u}_N)}\right]^T\in\mathbb{C}^{N\times 1},\\ \boldsymbol{t}^{\mathrm{SI}}_l(\boldsymbol{V})=\left[e^{-j\frac{2\pi}{\lambda}\rho^{\mathrm{SI}}_{\mathrm{t},l}(\boldsymbol{v}_1)},\ldots,e^{-j\frac{2\pi}{\lambda}\rho^{\mathrm{SI}}_{\mathrm{t},l}(\boldsymbol{v}_M)}\right]^T\in\mathbb{C}^{M\times 1},\end{cases} \tag{11}$$

where $\rho^{\mathrm{SI}}_{\mathrm{r},l}(\boldsymbol{u}_n)\triangleq x^{\mathrm{r}}_n\delta^{\mathrm{SI}}_{\mathrm{r},l}+y^{\mathrm{r}}_n\xi^{\mathrm{SI}}_{\mathrm{r},l}$ with $\delta^{\mathrm{SI}}_{\mathrm{r},l}=\sin\theta^{\mathrm{SI}}_{\mathrm{r},l}\cos\phi^{\mathrm{SI}}_{\mathrm{r},l}$ and $\xi^{\mathrm{SI}}_{\mathrm{r},l}=\cos\theta^{\mathrm{SI}}_{\mathrm{r},l}$, and $\rho^{\mathrm{SI}}_{\mathrm{t},l}(\boldsymbol{v}_m)\triangleq x^{\mathrm{t}}_m\delta^{\mathrm{SI}}_{\mathrm{t},l}+y^{\mathrm{t}}_m\xi^{\mathrm{SI}}_{\mathrm{t},l}$ with $\delta^{\mathrm{SI}}_{\mathrm{t},l}=$

$\sin\theta_{\mathrm{t},l}^{\mathrm{SI}}\cos\phi_{\mathrm{t},l}^{\mathrm{SI}}$ and $\xi_{\mathrm{t},l}^{\mathrm{SI}}=\cos\theta_{\mathrm{t},l}^{\mathrm{SI}}$. Let L_{SI} be the number of paths of the SI channel. Then, the SI channel is written as

$$\boldsymbol{H}_{\mathrm{SI}}(\boldsymbol{V},\boldsymbol{U})=\boldsymbol{R}_{\mathrm{SI}}(\boldsymbol{U})\boldsymbol{\Gamma}_{\mathrm{SI}}\boldsymbol{T}_{\mathrm{SI}}^{H}(\boldsymbol{V})\in\mathbb{C}^{N\times M}, \tag{12}$$

where $\boldsymbol{\Gamma}_{\mathrm{SI}}=\mathrm{diag}\{\gamma_{\mathrm{SI}}^{1},\ldots,\gamma_{\mathrm{SI}}^{L_{\mathrm{SI}}}\}\in\mathbb{C}^{L_{\mathrm{SI}}\times L_{\mathrm{SI}}}$ is the channel coefficient matrix, $\boldsymbol{R}_{\mathrm{SI}}(\boldsymbol{U})=\left[\boldsymbol{r}_{1}^{\mathrm{SI}}(\boldsymbol{U}),\ldots,\boldsymbol{r}_{L_{\mathrm{SI}}}^{\mathrm{SI}}(\boldsymbol{U})\right]\in\mathbb{C}^{N\times L_{\mathrm{SI}}}$, and $\boldsymbol{T}_{\mathrm{SI}}(\boldsymbol{V})=\left[\boldsymbol{t}_{1}^{\mathrm{SI}}(\boldsymbol{V}),\ldots,\boldsymbol{t}_{L_{\mathrm{SI}}}^{\mathrm{SI}}(\boldsymbol{V})\right]\in\mathbb{C}^{M\times L_{\mathrm{SI}}}$.

III. Problem Formulation

A. Communication Metric

According to (1), the SINR of the downlink user is

$$\eta_{\mathrm{d}}(\boldsymbol{V},\boldsymbol{w}_{\mathrm{t}})=\frac{\left|\boldsymbol{h}_{\mathrm{d}}(\boldsymbol{V})\boldsymbol{w}_{\mathrm{t}}\right|^{2}}{\sigma_{\mathrm{d}}^{2}}. \tag{13}$$

Similarly, the uplink communication SINR at the BS is

$$\eta_{\mathrm{u}}(\boldsymbol{\Phi})=\frac{p_{\mathrm{u}}\left|\boldsymbol{w}_{\mathrm{r}}^{H}\boldsymbol{h}_{\mathrm{u}}(\boldsymbol{U})\right|^{2}}{\left|\boldsymbol{w}_{\mathrm{r}}^{H}\boldsymbol{H}(\boldsymbol{V},\boldsymbol{U})\boldsymbol{w}_{\mathrm{t}}\right|^{2}+\sigma_{\mathrm{r}}^{2}\|\boldsymbol{w}_{\mathrm{r}}^{H}\|^{2}}, \tag{14}$$

where $\boldsymbol{w}_{\mathrm{r}}\in\mathbb{C}^{N\times 1}$ is the linear beamformer adopted by the BS for detecting s_{u}, $\boldsymbol{H}(\boldsymbol{V},\boldsymbol{U})=\boldsymbol{H}_{\mathrm{s}}(\boldsymbol{V},\boldsymbol{U})+\boldsymbol{H}_{\mathrm{SI}}(\boldsymbol{V},\boldsymbol{U})$, and $\boldsymbol{\Phi}=\{\boldsymbol{V},\boldsymbol{U},\boldsymbol{w}_{\mathrm{t}},\boldsymbol{w}_{\mathrm{r}},p_{\mathrm{u}}\}$ contains all the optimizing variables.

B. Sensing Metric

Since the detection probability is directly proportional to the sensing SINR [67], maximizing the sensing SINR has a direct effect of maximizing the detection probability. Therefore, we adopt the sensing SINR, given by

$$\eta_{\mathrm{s}}(\boldsymbol{\Phi})=\frac{\left|\boldsymbol{w}_{\mathrm{r}}^{H}\boldsymbol{H}_{\mathrm{s}}(\boldsymbol{V},\boldsymbol{U})\boldsymbol{w}_{\mathrm{t}}\right|^{2}}{p_{\mathrm{u}}\left|\boldsymbol{w}_{\mathrm{r}}^{H}\boldsymbol{h}_{\mathrm{u}}(\boldsymbol{U})\right|^{2}+\left|\boldsymbol{w}_{\mathrm{r}}^{H}\boldsymbol{H}_{\mathrm{SI}}(\boldsymbol{V},\boldsymbol{U})\boldsymbol{w}_{\mathrm{t}}\right|^{2}+\sigma_{\mathrm{r}}^{2}||\boldsymbol{w}_{\mathrm{r}}^{H}||^{2}}, \tag{15}$$

as the main sensing performance metric.

C. Optimization Problem

We aim to maximize the commmunication sum rate subject to a sensing SINR constraint by optimizing the transmit and receive antenna positions $\boldsymbol{V}$ and $\boldsymbol{U}$, the precoding and receive beamforming vectors $\boldsymbol{w}_{\mathrm{t}}$ and $\boldsymbol{w}_{\mathrm{r}}$, and the uplink transmit power p_{u}. Mathematically, this is formulated as

$$\begin{aligned}
\max_{\boldsymbol{\Phi}}\quad & f_{0}(\boldsymbol{\Phi})=\log\left(1+\eta_{\mathrm{d}}(\boldsymbol{V},\boldsymbol{w}_{\mathrm{t}})\right)+\log\left(1+\eta_{\mathrm{u}}(\boldsymbol{\Phi})\right)\\
\text{s.t.}\quad & \eta_{\mathrm{s}}(\boldsymbol{\Phi})\geq\eta,\\
& \|\boldsymbol{w}_{\mathrm{t}}\|^{2}\leq P_{\mathrm{t}},\\
& 0\leq p_{\mathrm{u}}\leq P_{\mathrm{u}},\\
& \boldsymbol{v}_{m},\boldsymbol{v}_{m'}\in\mathcal{S},\boldsymbol{v}_{m}\neq\boldsymbol{v}_{m'},\ \forall m,m'\in\mathcal{M},m\neq m',\\
& \boldsymbol{u}_{n},\boldsymbol{u}_{n'}\in\mathcal{S},\boldsymbol{u}_{n}\neq\boldsymbol{u}_{n'},\ \forall n,n'\in\mathcal{N},n\neq n',
\end{aligned} \tag{16}$$

where η is the sensing performance threshold, P_{t} and P_{u} are the power budgets of the BS and the uplink user, and $\mathcal{M}=\{1,\ldots,M\}$ and $\mathcal{N}=\{1,\ldots,N\}$ denote the index sets of the transmit and receive antennas, respectively.

IV. Proposed Solution

Problem (16) is non-convex and hence intractable. To proceed, we first remove $\boldsymbol{\Phi}$ from the log operation in the objective function $f_0(\boldsymbol{\Phi})$. Specifically, we introduce auxiliary variables $\boldsymbol{\Delta}=\{\Delta_{\mathrm{d}},\Delta_{\mathrm{u}}\}$ and transform $f_0(\boldsymbol{\Phi})$ to

$$\begin{aligned}
f_{1}(\boldsymbol{\Phi},\boldsymbol{\Delta})=&\log(1+\Delta_{\mathrm{d}})-\Delta_{\mathrm{d}}+\frac{(1+\Delta_{\mathrm{d}})\left|\boldsymbol{h}_{\mathrm{d}}(\boldsymbol{V})\boldsymbol{w}_{\mathrm{t}}\right|^{2}}{\left|\boldsymbol{h}_{\mathrm{d}}(\boldsymbol{V})\boldsymbol{w}_{\mathrm{t}}\right|^{2}+\sigma_{\mathrm{d}}^{2}}+\log(1+\Delta_{\mathrm{u}})\\
&-\Delta_{\mathrm{u}}+\frac{(1+\Delta_{\mathrm{u}})p_{\mathrm{u}}\left|\boldsymbol{w}_{\mathrm{r}}^{H}\boldsymbol{h}_{\mathrm{u}}(\boldsymbol{U})\right|^{2}}{p_{\mathrm{u}}|\boldsymbol{w}_{\mathrm{r}}^{H}\boldsymbol{h}_{\mathrm{u}}(\boldsymbol{U})|^{2}+|\boldsymbol{w}_{\mathrm{r}}^{H}\boldsymbol{H}(\boldsymbol{V},\boldsymbol{U})\boldsymbol{w}_{\mathrm{t}}|^{2}+\sigma_{\mathrm{r}}^{2}\|\boldsymbol{w}_{\mathrm{r}}^{H}\|^{2}}.
\end{aligned} \tag{17}$$

For fixed $\boldsymbol{\Phi}$, by setting $\frac{\partial f_1}{\partial\Delta_{\mathrm{d}}}$ and $\frac{\partial f_1}{\partial\Delta_{\mathrm{u}}}$ to zero, we have

$$\begin{cases}
\Delta_{\mathrm{d}}^{*}=\dfrac{\left|\boldsymbol{h}_{\mathrm{d}}(\boldsymbol{V})\boldsymbol{w}_{\mathrm{t}}\right|^{2}}{\sigma_{\mathrm{d}}^{2}},\\
\Delta_{\mathrm{u}}^{*}=\dfrac{p_{\mathrm{u}}\left|\boldsymbol{w}_{\mathrm{r}}^{H}\boldsymbol{h}_{\mathrm{u}}(\boldsymbol{U})\right|^{2}}{\left|\boldsymbol{w}_{\mathrm{r}}^{H}\boldsymbol{H}(\boldsymbol{V},\boldsymbol{U})\boldsymbol{w}_{\mathrm{t}}\right|^{2}+\sigma_{\mathrm{r}}^{2}\|\boldsymbol{w}_{\mathrm{r}}^{H}\|^{2}}.
\end{cases} \tag{18}$$

It is easy to prove that $f_1(\boldsymbol{\Phi},\boldsymbol{\Delta}^{*})=f_0(\boldsymbol{\Phi})$. Therefore, (16) can be equivalently transformed to

$$\begin{aligned}
\max_{\boldsymbol{\Phi},\boldsymbol{\Delta}}\quad & f_{1}(\boldsymbol{\Phi},\boldsymbol{\Delta})\\
\text{s.t.}\quad & f_{\mathrm{s}}(\boldsymbol{\Phi})\geq 0,\\
& \|\boldsymbol{w}_{\mathrm{t}}\|^{2}\leq P_{\mathrm{t}},\\
& 0\leq p_{\mathrm{u}}\leq P_{\mathrm{u}},\\
& \boldsymbol{v}_{m},\boldsymbol{v}_{m'}\in\mathcal{S},\boldsymbol{v}_{m}\neq\boldsymbol{v}_{m'},\ \forall m,m'\in\mathcal{M},m\neq m',\\
& \boldsymbol{u}_{n},\boldsymbol{u}_{n'}\in\mathcal{S},\boldsymbol{u}_{n}\neq\boldsymbol{u}_{n'},\ \forall n,n'\in\mathcal{N},n\neq n',
\end{aligned} \tag{19}$$

where $f_{\mathrm{s}}(\boldsymbol{\Phi})=\left|\boldsymbol{w}_{\mathrm{r}}^{H}\boldsymbol{H}_{\mathrm{s}}(\boldsymbol{V},\boldsymbol{U})\boldsymbol{w}_{\mathrm{t}}\right|^{2}-\eta\Big(p_{\mathrm{u}}\left|\boldsymbol{w}_{\mathrm{r}}^{H}\boldsymbol{h}_{\mathrm{u}}(\boldsymbol{U})\right|^{2}+\left|\boldsymbol{w}_{\mathrm{r}}^{H}\boldsymbol{H}_{\mathrm{SI}}(\boldsymbol{V},\boldsymbol{U})\boldsymbol{w}_{\mathrm{t}}\right|^{2}+\sigma_{\mathrm{r}}^{2}||\boldsymbol{w}_{\mathrm{r}}^{H}||^{2}\Big)$. To deal with the fractional terms in $f_1(\boldsymbol{\Phi},\boldsymbol{\Delta})$, we further introduce auxiliary variables $\boldsymbol{\omega}=\{\omega_{\mathrm{d}},\omega_{\mathrm{u}}\}$ as in [68], [69] to reformulate $f_1(\boldsymbol{\Phi},\boldsymbol{\Delta})$ as

$$\begin{aligned}
f_{2}(\boldsymbol{\Phi},\boldsymbol{\Delta},\boldsymbol{\omega})=&\log(1+\Delta_{\mathrm{d}})-\Delta_{\mathrm{d}}\\
&+(1+\Delta_{\mathrm{d}})\Big[2\mathrm{Re}\{\omega_{\mathrm{d}}^{H}\boldsymbol{h}_{\mathrm{d}}(\boldsymbol{V})\boldsymbol{w}_{\mathrm{t}}\}-|\omega_{\mathrm{d}}|^{2}\left(|\boldsymbol{h}_{\mathrm{d}}(\boldsymbol{V})\boldsymbol{w}_{\mathrm{t}}|^{2}+\sigma_{\mathrm{d}}^{2}\right)\Big]\\
&+\log(1+\Delta_{\mathrm{u}})-\Delta_{\mathrm{u}}+p_{\mathrm{u}}(1+\Delta_{\mathrm{u}})\Big[2\mathrm{Re}\{\omega_{\mathrm{u}}^{H}\boldsymbol{w}_{\mathrm{r}}^{H}\boldsymbol{h}_{\mathrm{u}}(\boldsymbol{U})\}\\
&-|\omega_{\mathrm{u}}|^{2}\left(p_{\mathrm{u}}\left|\boldsymbol{w}_{\mathrm{r}}^{H}\boldsymbol{h}_{\mathrm{u}}(\boldsymbol{U})\right|^{2}+\left|\boldsymbol{w}_{\mathrm{r}}^{H}\boldsymbol{H}(\boldsymbol{V},\boldsymbol{U})\boldsymbol{w}_{\mathrm{t}}\right|^{2}+\sigma_{\mathrm{r}}^{2}\|\boldsymbol{w}_{\mathrm{r}}^{H}\|^{2}\right)\Big].
\end{aligned} \tag{20}$$

By setting $\frac{\partial f_2}{\partial\omega_{\mathrm{d}}}$ and $\frac{\partial f_2}{\partial\omega_{\mathrm{u}}}$ to zero, we can obtain the optimal value of $f_2(\boldsymbol{\Phi},\boldsymbol{\Delta},\boldsymbol{\omega})$ at

$$\begin{cases}
\omega_{\mathrm{d}}^{*}=\dfrac{\boldsymbol{h}_{\mathrm{d}}(\boldsymbol{V})\boldsymbol{w}_{\mathrm{t}}}{\left|\boldsymbol{h}_{\mathrm{d}}(\boldsymbol{V})\boldsymbol{w}_{\mathrm{t}}\right|^{2}+\sigma_{\mathrm{d}}^{2}},\\
\omega_{\mathrm{u}}^{*}=\dfrac{\boldsymbol{w}_{\mathrm{r}}^{H}\boldsymbol{h}_{\mathrm{u}}(\boldsymbol{U})}{p_{\mathrm{u}}|\boldsymbol{w}_{\mathrm{r}}^{H}\boldsymbol{h}_{\mathrm{u}}(\boldsymbol{U})|^{2}+|\boldsymbol{w}_{\mathrm{r}}^{H}\boldsymbol{H}(\boldsymbol{V},\boldsymbol{U})\boldsymbol{w}_{\mathrm{t}}|^{2}+\sigma_{\mathrm{r}}^{2}\|\boldsymbol{w}_{\mathrm{r}}^{H}\|^{2}}.
\end{cases} \tag{21}$$

Since $f_2(\boldsymbol{\Phi},\boldsymbol{\Delta},\boldsymbol{\omega}^*)=f_1(\boldsymbol{\Phi},\boldsymbol{\Delta})$, (19) can be recast as

$$\begin{aligned}\max_{\boldsymbol{\Phi},\boldsymbol{\Delta},\boldsymbol{\omega}}\quad & f_2(\boldsymbol{\Phi},\boldsymbol{\Delta},\boldsymbol{\omega})\\ \text{s.t.}\quad & f_{\mathrm{s}}(\boldsymbol{\Phi})\geq 0,\\ & \|\boldsymbol{w}_{\mathrm{t}}\|^2\leq P_{\mathrm{t}},\\ & 0\leq p_{\mathrm{u}}\leq P_{\mathrm{u}},\\ & \boldsymbol{v}_m,\boldsymbol{v}_{m'}\in\mathcal{S},\boldsymbol{v}_m\neq\boldsymbol{v}_{m'},\ \forall m,m'\in\mathcal{M},m\neq m',\\ & \boldsymbol{u}_n,\boldsymbol{u}_{n'}\in\mathcal{S},\boldsymbol{u}_n\neq\boldsymbol{u}_{n'},\ \forall n,n'\in\mathcal{N},n\neq n'.\end{aligned}\tag{22}$$

Though (22) is much simpler than (16), it is still hard. In the sequel, we iteratively update each variable while considering others fixed. For notation convenience, when $\boldsymbol{V}$ and $\boldsymbol{U}$ are fixed, we omit them from the channel variables, e.g., we denote $\boldsymbol{h}_{\mathrm{d}}(\boldsymbol{V})$ and $\boldsymbol{h}_{\mathrm{u}}(\boldsymbol{U})$ as $\boldsymbol{h}_{\mathrm{d}}$ and $\boldsymbol{h}_{\mathrm{u}}$, respectively.

A. Updating Auxiliary Variables

According to the FP framework, we find the optimal values of $\boldsymbol{\Delta}$ and $\boldsymbol{\omega}$ based on (18) and (21), respectively.

B. Updating Transmit Beamforming Vector

Here, we aim to solve the sub-problem of optimizing $\boldsymbol{w}_{\mathrm{t}}$. With fixed $\{\boldsymbol{V},\boldsymbol{U},\boldsymbol{w}_{\mathrm{r}},p_{\mathrm{u}},\boldsymbol{\Delta},\boldsymbol{\omega}\}$, (22) reduces to

$$\max_{\boldsymbol{w}_{\mathrm{t}}}\quad -\boldsymbol{w}_{\mathrm{t}}^H\boldsymbol{\phi}_1\boldsymbol{w}_{\mathrm{t}}+\mu_1\mathrm{Re}\{\omega_{\mathrm{d}}^H\boldsymbol{h}_{\mathrm{d}}\boldsymbol{w}_{\mathrm{t}}\}\tag{23a}$$

$$\text{s.t.}\quad \boldsymbol{w}_{\mathrm{t}}^H\boldsymbol{\phi}_2\boldsymbol{w}_{\mathrm{t}}-\boldsymbol{w}_{\mathrm{t}}^H\boldsymbol{\phi}_3\boldsymbol{w}_{\mathrm{t}}+\mu_2\leq 0,\tag{23b}$$

$$\|\boldsymbol{w}_{\mathrm{t}}\|^2\leq P_{\mathrm{t}},\tag{23c}$$

where $\mu_1=2(1+\Delta_{\mathrm{d}})$, $\boldsymbol{\phi}_1=(1+\Delta_{\mathrm{d}})|\omega_{\mathrm{d}}|^2\boldsymbol{h}_{\mathrm{d}}^H\boldsymbol{h}_{\mathrm{d}}+p_{\mathrm{u}}(1+\Delta_{\mathrm{u}})|\omega_{\mathrm{u}}|^2\boldsymbol{H}^H\boldsymbol{w}_{\mathrm{r}}\boldsymbol{w}_{\mathrm{r}}^H\boldsymbol{H}$, $\boldsymbol{\phi}_2=\eta\boldsymbol{H}_{\mathrm{SI}}^H\boldsymbol{w}_{\mathrm{r}}\boldsymbol{w}_{\mathrm{r}}^H\boldsymbol{H}_{\mathrm{SI}}$, $\boldsymbol{\phi}_3=\boldsymbol{H}_{\mathrm{s}}^H\boldsymbol{w}_{\mathrm{r}}\boldsymbol{w}_{\mathrm{r}}^H\boldsymbol{H}_{\mathrm{s}}$, and $\mu_2=\eta\left(p_{\mathrm{u}}\left|\boldsymbol{w}_{\mathrm{r}}^H\boldsymbol{h}_{\mathrm{u}}\right|^2+\sigma_{\mathrm{r}}^2\|\boldsymbol{w}_{\mathrm{r}}^H\|^2\right)$. Since (23b) is in the difference of convex (DC) form, we apply the MM framework to iteratively optimize $\boldsymbol{w}_{\mathrm{t}}$. In particular, a lower-bound of $\boldsymbol{w}_{\mathrm{t}}^H\boldsymbol{\phi}_3\boldsymbol{w}_{\mathrm{t}}$ can be constructed through the Taylor series expansion, given by

$$\boldsymbol{w}_{\mathrm{t}}^H\boldsymbol{\phi}_3\boldsymbol{w}_{\mathrm{t}}\geq 2\mathrm{Re}\{\boldsymbol{w}_{\mathrm{t},0}^H\boldsymbol{\phi}_3(\boldsymbol{w}_{\mathrm{t}}-\boldsymbol{w}_{\mathrm{t},0})\}+\boldsymbol{w}_{\mathrm{t},0}^H\boldsymbol{\phi}_3\boldsymbol{w}_{\mathrm{t},0},\tag{24}$$

where $\boldsymbol{w}_{\mathrm{t},0}$ is the value of $\boldsymbol{w}_{\mathrm{t}}$ in the previous iteration. Then (23) can be rewritten as

$$\begin{aligned}\max_{\boldsymbol{w}_{\mathrm{t}}}\quad & -\boldsymbol{w}_{\mathrm{t}}^H\boldsymbol{\phi}_1\boldsymbol{w}_{\mathrm{t}}+\mu_1\mathrm{Re}\{\omega_{\mathrm{d}}^H\boldsymbol{h}_{\mathrm{d}}\boldsymbol{w}_{\mathrm{t}}\}\\ \text{s.t.}\quad & \boldsymbol{w}_{\mathrm{t}}^H\boldsymbol{\phi}_2\boldsymbol{w}_{\mathrm{t}}-2\mathrm{Re}\{\boldsymbol{w}_{\mathrm{t},0}^H\boldsymbol{\phi}_3\boldsymbol{w}_{\mathrm{t}}\}+\mu_3\leq 0,\\ & \|\boldsymbol{w}_{\mathrm{t}}\|^2\leq P_{\mathrm{t}},\end{aligned}\tag{25}$$

where $\mu_3=\mu_2+\boldsymbol{w}_{\mathrm{t},0}^H\boldsymbol{\phi}_3\boldsymbol{w}_{\mathrm{t},0}$. Obviously, problem (25) is a QCQP and thus can be solved by CVX.

C. Updating Receive Beamforming Vector

Now, we deal with the sub-problem of optimizing $\boldsymbol{w}_{\mathrm{r}}$. With fixed $\{\boldsymbol{V},\boldsymbol{U},\boldsymbol{w}_{\mathrm{t}},p_{\mathrm{u}},\boldsymbol{\Delta},\boldsymbol{\omega}\}$, problem (22) becomes

$$\begin{aligned}\max_{\boldsymbol{w}_{\mathrm{r}}}\quad & -\boldsymbol{w}_{\mathrm{r}}^H\boldsymbol{\psi}_1\boldsymbol{w}_{\mathrm{r}}+2\mathrm{Re}\{\omega_{\mathrm{u}}^H\boldsymbol{w}_{\mathrm{r}}^H\boldsymbol{h}_{\mathrm{u}}\}\\ \text{s.t.}\quad & \boldsymbol{w}_{\mathrm{r}}^H\boldsymbol{\psi}_2\boldsymbol{w}_{\mathrm{r}}-\boldsymbol{w}_{\mathrm{r}}^H\boldsymbol{\psi}_3\boldsymbol{w}_{\mathrm{r}}\leq 0,\end{aligned}\tag{26}$$

where $\boldsymbol{\psi}_1=|\omega_{\mathrm{u}}|^2(p_{\mathrm{u}}\boldsymbol{h}_{\mathrm{u}}\boldsymbol{h}_{\mathrm{u}}^H+\boldsymbol{H}\boldsymbol{w}_{\mathrm{t}}\boldsymbol{w}_{\mathrm{t}}^H\boldsymbol{H}^H+\sigma_{\mathrm{r}}^2\boldsymbol{I})$, $\boldsymbol{\psi}_2=\eta(p_{\mathrm{u}}\boldsymbol{h}_{\mathrm{u}}\boldsymbol{h}_{\mathrm{u}}^H+\boldsymbol{H}_{\mathrm{SI}}\boldsymbol{w}_{\mathrm{t}}\boldsymbol{w}_{\mathrm{t}}^H\boldsymbol{H}_{\mathrm{SI}}^H+\sigma_{\mathrm{r}}^2\boldsymbol{I})$, and $\boldsymbol{\psi}_3=\boldsymbol{H}_{\mathrm{s}}\boldsymbol{w}_{\mathrm{t}}\boldsymbol{w}_{\mathrm{t}}^H\boldsymbol{H}_{\mathrm{s}}^H$. Note that (26) has the same form as (23). Therefore, it can also be transformed into a QCQP and solved by CVX.

D. Updating Uplink Transmit Power

Next, we address the sub-problem related to p_{u}. With fixed $\{\boldsymbol{V},\boldsymbol{U},\boldsymbol{w}_{\mathrm{t}},\boldsymbol{w}_{\mathrm{r}},\boldsymbol{\Delta},\boldsymbol{\omega}\}$, (22) becomes

$$\begin{aligned}\max_{p_{\mathrm{u}}}\quad & -\alpha_1p_{\mathrm{u}}^2+\alpha_2p_{\mathrm{u}}\\ \text{s.t.}\quad & p_{\mathrm{u}}\leq\alpha_3,\\ & 0\leq p_{\mathrm{u}}\leq P_{\mathrm{u}},\end{aligned}\tag{27}$$

where $\alpha_1=|\omega_{\mathrm{u}}|^2|\boldsymbol{w}_{\mathrm{r}}^H\boldsymbol{h}_{\mathrm{u}}|^2$, $\alpha_2=2\mathrm{Re}\{\omega_{\mathrm{u}}^H\boldsymbol{w}_{\mathrm{r}}^H\boldsymbol{h}_{\mathrm{u}}\}-|\omega_{\mathrm{u}}|^2\left(\left|\boldsymbol{w}_{\mathrm{r}}^H\boldsymbol{H}\boldsymbol{w}_{\mathrm{t}}\right|^2+\sigma_{\mathrm{r}}^2\|\boldsymbol{w}_{\mathrm{r}}^H\|^2\right)$, and $\alpha_3=\Big[\left|\boldsymbol{w}_{\mathrm{r}}^H\boldsymbol{H}_{\mathrm{s}}\boldsymbol{w}_{\mathrm{t}}\right|^2-\eta\left(\left|\boldsymbol{w}_{\mathrm{r}}^H\boldsymbol{H}_{\mathrm{SI}}\boldsymbol{w}_{\mathrm{t}}\right|^2+\sigma_{\mathrm{r}}^2\|\boldsymbol{w}_{\mathrm{r}}^H\|^2\right)\Big]/\left(\eta\left|\boldsymbol{w}_{\mathrm{r}}^H\boldsymbol{h}_{\mathrm{u}}\right|^2\right)$. Obviously, problem (27) is feasible only when $\alpha_3\geq 0$. If $\alpha_3\geq 0$ and $\alpha_1=0$, the optimal solution of the problem can be reached at $p_{\mathrm{u}}=0$ if $\alpha_2\leq 0$, or at $p_{\mathrm{u}}=\min\{\alpha_3,P_{\mathrm{u}}\}$ if $\alpha_2>0$. If $\alpha_3\geq 0$ and $\alpha_1>0$, the objective function of (27) is a parabola with a downward opening. Then, it is easy to verify that for $\alpha_3\geq 0$ and $\alpha_1>0$, the optimal value of p_{u} is given by

$$p_{\mathrm{u}}^*=\min\left\{\max\left\{\frac{\alpha_2}{2\alpha_1},0\right\},\min\{\alpha_3,P_{\mathrm{u}}\}\right\}.\tag{28}$$

E. Updating Transmit Antenna Positions

In this subsection, we solve the sub-problem of optimizing $\boldsymbol{V}$ using the proposed theorems and the SCA algorithm. With fixed $\{\boldsymbol{U},\boldsymbol{w}_{\mathrm{t}},\boldsymbol{w}_{\mathrm{r}},p_{\mathrm{u}},\boldsymbol{\Delta},\boldsymbol{\omega}\}$, problem (22) becomes

$$\begin{aligned}\max_{\boldsymbol{V}}\quad & \alpha_d\Big(2\mathrm{Re}\{\omega_{\mathrm{d}}^H\boldsymbol{h}_{\mathrm{d}}(\boldsymbol{V})\boldsymbol{w}_{\mathrm{t}}\}-|\omega_{\mathrm{d}}|^2\left|\boldsymbol{h}_{\mathrm{d}}(\boldsymbol{V})\boldsymbol{w}_{\mathrm{t}}\right|^2\Big)\\ & -\alpha_u\left|\boldsymbol{w}_{\mathrm{r}}^H\boldsymbol{H}(\boldsymbol{V})\boldsymbol{w}_{\mathrm{t}}\right|^2\\ \text{s.t.}\quad & \left|\boldsymbol{w}_{\mathrm{r}}^H\boldsymbol{H}_{\mathrm{s}}(\boldsymbol{V})\boldsymbol{w}_{\mathrm{t}}\right|^2-\eta\left|\boldsymbol{w}_{\mathrm{r}}^H\boldsymbol{H}_{\mathrm{SI}}(\boldsymbol{V})\boldsymbol{w}_{\mathrm{t}}\right|^2\geq\beta_1,\\ & \boldsymbol{v}_m,\boldsymbol{v}_{m'}\in\mathcal{S},\boldsymbol{v}_m\neq\boldsymbol{v}_{m'},\ \forall m,m\in\mathcal{M},m\neq m',\end{aligned}\tag{29}$$

where $\alpha_d=1+\Delta_{\mathrm{d}}$, $\alpha_u=p_u(1+\Delta_{\mathrm{u}})|\omega_{\mathrm{u}}|^2$, and $\beta_1=\eta\left(p_{\mathrm{u}}\left|\boldsymbol{w}_{\mathrm{r}}^H\boldsymbol{h}_{\mathrm{u}}\right|^2+\sigma_{\mathrm{r}}^2\|\boldsymbol{w}_{\mathrm{r}}^H\|^2\right)$. Denoting $\boldsymbol{T}_{\mathrm{s}}(\boldsymbol{V})=\boldsymbol{a}_{\mathrm{t}}(\boldsymbol{V})$ and considering the model in Section II-B, (29) is rewritten as

$$\begin{aligned}\max_{\boldsymbol{V}}\ & \alpha_d\Big(2\mathrm{Re}\{\omega_{\mathrm{d}}^H\boldsymbol{1}^H\boldsymbol{\Gamma}_{\mathrm{d}}\boldsymbol{T}_{\mathrm{d}}^H(\boldsymbol{V})\boldsymbol{w}_{\mathrm{t}}\}-|\omega_{\mathrm{d}}|^2\left|\boldsymbol{1}^H\boldsymbol{\Gamma}_{\mathrm{d}}\boldsymbol{T}_{\mathrm{d}}^H(\boldsymbol{V})\boldsymbol{w}_{\mathrm{t}}\right|^2\Big)\\ & -\alpha_u\Big(\left|\alpha_{\mathrm{s}}\boldsymbol{w}_{\mathrm{r}}^H\boldsymbol{a}_{\mathrm{r}}\boldsymbol{T}_{\mathrm{s}}^H(\boldsymbol{V})\boldsymbol{w}_{\mathrm{t}}\right|^2+\left|\boldsymbol{w}_{\mathrm{r}}^H\boldsymbol{R}_{\mathrm{SI}}\boldsymbol{\Gamma}_{\mathrm{SI}}\boldsymbol{T}_{\mathrm{SI}}^H(\boldsymbol{V})\boldsymbol{w}_{\mathrm{t}}\right|^2\\ & +2\mathrm{Re}\{\left(\alpha_{\mathrm{s}}\boldsymbol{w}_{\mathrm{r}}^H\boldsymbol{a}_{\mathrm{r}}\boldsymbol{T}_{\mathrm{s}}^H(\boldsymbol{V})\boldsymbol{w}_{\mathrm{t}}\right)\left(\boldsymbol{w}_{\mathrm{r}}^H\boldsymbol{R}_{\mathrm{SI}}\boldsymbol{\Gamma}_{\mathrm{SI}}\boldsymbol{T}_{\mathrm{SI}}^H(\boldsymbol{V})\boldsymbol{w}_{\mathrm{t}}\right)^H\}\Big)\\ \text{s.t.}\ & \eta\left|\boldsymbol{w}_{\mathrm{r}}^H\boldsymbol{R}_{\mathrm{SI}}\boldsymbol{\Gamma}_{\mathrm{SI}}\boldsymbol{T}_{\mathrm{SI}}^H(\boldsymbol{V})\boldsymbol{w}_{\mathrm{t}}\right|^2-\left|\alpha_{\mathrm{s}}\boldsymbol{w}_{\mathrm{r}}^H\boldsymbol{a}_{\mathrm{r}}\boldsymbol{T}_{\mathrm{s}}^H(\boldsymbol{V})\boldsymbol{w}_{\mathrm{t}}\right|^2\leq-\beta_1,\\ & \boldsymbol{v}_m,\boldsymbol{v}_{m'}\in\mathcal{S},\boldsymbol{v}_m\neq\boldsymbol{v}_{m'},\ \forall m,m\in\mathcal{M},m\neq m'.\end{aligned}\tag{30}$$

Since the problem is still non-convex and difficult to solve, we resort to SCA. For convenience, denote $\boldsymbol{v}=\mathrm{vector}\{\boldsymbol{V}\}=[x_1^{\mathrm{t}},\ldots,x_M^{\mathrm{t}},y_1^{\mathrm{t}},\ldots,y_M^{\mathrm{t}}]^T=[v_1,\ldots,v_{2M}]^T$.

Theorem 1. *For arbitrary vectors $\boldsymbol{a}=[a_1,\ldots,a_L]^T$ and $\boldsymbol{b}=[b_1,\ldots,b_M]^T$, $\boldsymbol{v}^T\hat{\boldsymbol{\Lambda}}\boldsymbol{v}+\hat{\boldsymbol{c}}\boldsymbol{v}+\hat{d}$ and $-\boldsymbol{v}^T\hat{\boldsymbol{\Lambda}}\boldsymbol{v}+\bar{\boldsymbol{c}}\boldsymbol{v}+\bar{d}$ are concave and convex quadratic surrogate functions for $|\boldsymbol{a}^T\boldsymbol{T}_{\chi_1}^H(\boldsymbol{V})\boldsymbol{b}|^2$ respectively, where $\chi_1\in\{\mathrm{d},\mathrm{SI},\mathrm{s}\}$, $\hat{\boldsymbol{\Lambda}}$, $\hat{\boldsymbol{c}}$, and $\hat{d}$ are given in (53), while $\bar{\boldsymbol{c}}$ and $\bar{d}$ are given in (56), and $\hat{\boldsymbol{\Lambda}}$ is a negative semi-definite (NSD) matrix.*

Proof: See Appendix A. ∎

Based on Theorem 1, a concave quadratic surrogate function of $\left|\alpha_{\mathrm{s}}\boldsymbol{w}_{\mathrm{r}}^H\boldsymbol{a}_{\mathrm{r}}\boldsymbol{T}_{\mathrm{s}}^H(\boldsymbol{V})\boldsymbol{w}_{\mathrm{t}}\right|^2$ can be obtained as

$$\boldsymbol{v}^T\hat{\boldsymbol{\Lambda}}_{\mathrm{s}}\boldsymbol{v}+\hat{\boldsymbol{c}}_{\mathrm{s}}\boldsymbol{v}+\hat{d}_{\mathrm{s}}. \tag{31}$$

Moreover, we can obtain the convex quadratic surrogate functions of $\left|\mathbf{1}^H\boldsymbol{\Gamma}_{\mathrm{d}}\boldsymbol{T}_{\mathrm{d}}^H(\boldsymbol{V})\boldsymbol{w}_{\mathrm{t}}\right|^2$, $\left|\alpha_{\mathrm{s}}\boldsymbol{w}_{\mathrm{r}}^H\boldsymbol{a}_{\mathrm{r}}\boldsymbol{T}_{\mathrm{s}}^H(\boldsymbol{V})\boldsymbol{w}_{\mathrm{t}}\right|^2$, and $\left|\boldsymbol{w}_{\mathrm{r}}^H\boldsymbol{R}_{\mathrm{SI}}\boldsymbol{\Gamma}_{\mathrm{SI}}\boldsymbol{T}_{\mathrm{SI}}^H(\boldsymbol{V})\boldsymbol{w}_{\mathrm{t}}\right|^2$ as

$$-\boldsymbol{v}^T\hat{\boldsymbol{\Lambda}}_{\mathrm{d}}\boldsymbol{v}+\bar{\boldsymbol{c}}_{\mathrm{d}}\boldsymbol{v}+\bar{d}_{\mathrm{d}}, \tag{32}$$
$$-\boldsymbol{v}^T\hat{\boldsymbol{\Lambda}}_{\mathrm{s}}\boldsymbol{v}+\bar{\boldsymbol{c}}_{\mathrm{s}}\boldsymbol{v}+\bar{d}_{\mathrm{s}}, \tag{33}$$
$$-\boldsymbol{v}^T\hat{\boldsymbol{\Lambda}}_{\mathrm{SI}}\boldsymbol{v}+\bar{\boldsymbol{c}}_{\mathrm{SI}}\boldsymbol{v}+\bar{d}_{\mathrm{SI}}. \tag{34}$$

Theorem 2. *For any $\boldsymbol{a}\in\mathbb{C}^{L\times1}$ and $\boldsymbol{b}\in\mathbb{C}^{M\times1}$, a concave quadratic surrogate function for $\mathrm{Re}\{\boldsymbol{a}^T\boldsymbol{T}_{\chi_1}^H(\boldsymbol{V})\boldsymbol{b}\}$ is given by $\boldsymbol{v}^T\tilde{\boldsymbol{\Lambda}}\boldsymbol{v}+\tilde{\boldsymbol{c}}\boldsymbol{v}+\tilde{d}$, where $\chi_1\in\{\mathrm{d},\mathrm{SI},\mathrm{s}\}$, and $\tilde{\boldsymbol{\Lambda}}$ is an NSD matrix defined in (59) along with $\tilde{\boldsymbol{c}}$ and $\tilde{d}$.*

Proof: See Appendix B. ∎

According to Theorem 2, a concave quadratic surrogate function of $\mathrm{Re}\{\omega_{\mathrm{d}}^H\mathbf{1}^H\boldsymbol{\Gamma}_{\mathrm{d}}\boldsymbol{T}_{\mathrm{d}}^H(\boldsymbol{V})\boldsymbol{w}_{\mathrm{t}}\}$ can be written as

$$\boldsymbol{v}^T\tilde{\boldsymbol{\Lambda}}_{\mathrm{d}}\boldsymbol{v}+\tilde{\boldsymbol{c}}_{\mathrm{d}}\boldsymbol{v}+\tilde{d}_{\mathrm{d}}. \tag{35}$$

Theorem 3. *For any vectors $\boldsymbol{a}=[a_1,\ldots,a_L]^T$, $\boldsymbol{b}=[b_1,\ldots,b_M]^T$, and $\check{\boldsymbol{a}}=[\check{a}_1,\ldots,\check{a}_{\check{L}}]^T$, a convex quadratic surrogate function for $\mathrm{Re}\{\left(\boldsymbol{a}^T\boldsymbol{T}_{\chi}^H(\boldsymbol{V})\boldsymbol{b}\right)\left(\check{\boldsymbol{a}}^T\boldsymbol{T}_{\check{\chi}}^H(\boldsymbol{V})\boldsymbol{b}\right)^H\}$ can be expressed as $\boldsymbol{v}^T\check{\boldsymbol{\Lambda}}\boldsymbol{v}+\check{\boldsymbol{c}}\boldsymbol{v}+\check{d}$, where $\chi,\check{\chi}\in\{\mathrm{d},\mathrm{SI},\mathrm{s}\}$, $\chi\neq\check{\chi}$, $\check{\boldsymbol{\Lambda}}$ is a positive semi-definite (PSD) matrix, and $\check{\boldsymbol{\Lambda}}$, $\check{\boldsymbol{c}}$, $\check{d}$ are given in (63).*

Proof: See Appendix C. ∎

Then we denote the convex quadratic surrogate function for $\mathrm{Re}\{\left(\alpha_{\mathrm{s}}\boldsymbol{w}_{\mathrm{r}}^H\boldsymbol{a}_{\mathrm{r}}\boldsymbol{T}_{\mathrm{s}}^H(\boldsymbol{V})\boldsymbol{w}_{\mathrm{t}}\right)\left(\boldsymbol{w}_{\mathrm{r}}^H\boldsymbol{R}_{\mathrm{SI}}\boldsymbol{\Gamma}_{\mathrm{SI}}\boldsymbol{T}_{\mathrm{SI}}^H(\boldsymbol{V})\boldsymbol{w}_{\mathrm{t}}\right)^H\}$ using Theorem 3 as

$$\boldsymbol{v}^T\check{\boldsymbol{\Lambda}}_{\mathrm{sSI}}\boldsymbol{v}+\check{\boldsymbol{c}}_{\mathrm{sSI}}\boldsymbol{v}+\check{d}_{\mathrm{sSI}}. \tag{36}$$

Denoting $\boldsymbol{\Lambda}_1=\alpha_{\mathrm{d}}(2\tilde{\boldsymbol{\Lambda}}_{\mathrm{d}}+|\omega_{\mathrm{d}}|^2\hat{\boldsymbol{\Lambda}}_{\mathrm{d}})+\alpha_{\mathrm{u}}(\hat{\boldsymbol{\Lambda}}_{\mathrm{s}}+\hat{\boldsymbol{\Lambda}}_{\mathrm{SI}}-2\check{\boldsymbol{\Lambda}}_{\mathrm{sSI}})$, $\boldsymbol{c}_1=\alpha_{\mathrm{d}}(2\tilde{\boldsymbol{c}}_{\mathrm{d}}-|\omega_{\mathrm{d}}|^2\bar{\boldsymbol{c}}_{\mathrm{d}})-\alpha_{\mathrm{u}}(\bar{\boldsymbol{c}}_{\mathrm{s}}+\bar{\boldsymbol{c}}_{\mathrm{SI}}+2\check{\boldsymbol{c}}_{\mathrm{sSI}})$, $d_1=\alpha_{\mathrm{d}}(2\tilde{d}_{\mathrm{d}}-|\omega_{\mathrm{d}}|^2\bar{d}_{\mathrm{d}})-\alpha_{\mathrm{u}}(\bar{d}_{\mathrm{s}}+\bar{d}_{\mathrm{SI}}+2\check{d}_{\mathrm{sSI}})$, $\boldsymbol{\Lambda}_2=-\eta\hat{\boldsymbol{\Lambda}}_{\mathrm{SI}}-\hat{\boldsymbol{\Lambda}}_{\mathrm{s}}$, $\boldsymbol{c}_2=\eta\bar{\boldsymbol{c}}_{\mathrm{SI}}-\hat{\boldsymbol{c}}_{\mathrm{s}}$, and $d_2=\eta\bar{d}_{\mathrm{SI}}-\hat{d}_{\mathrm{s}}$, (30) can be transformed to

$$\max_{\boldsymbol{v}}\quad \boldsymbol{v}^T\boldsymbol{\Lambda}_1\boldsymbol{v}+\boldsymbol{c}_1\boldsymbol{v}+d_1, \tag{37a}$$
$$\text{s.t.}\quad \boldsymbol{v}^T\boldsymbol{\Lambda}_2\boldsymbol{v}+\boldsymbol{c}_2\boldsymbol{v}+d_2\leq-\beta_1, \tag{37b}$$
$$0\leq v_m\leq W, m=1,\ldots,2M, \tag{37c}$$
$$[v_m,v_{m+M}]\neq[v_{m'},v_{m'+M}],\ \forall m,m'\in\mathcal{M},m\neq m'. \tag{37d}$$

Without (37d), (37) is convex and can be solved by CVX. Noting that in Theorems 1, 2, and 3, the quadratic surrogate functions are based on the Taylor series expansion in the given antenna positions $\boldsymbol{V}_0$, we apply the SCA method to solve (29). Specifically, we start SCA from valid $\boldsymbol{v}$ that satisfies (37d), and then update $\boldsymbol{v}$ only if it satisfies (37d) in each iteration. The main steps of solving (29) are summarized in Algorithm 1.

Algorithm 1 SCA-based algorithm for solving (29)

Initialize $\boldsymbol{V}_0$ by randomly generating antenna positions that satisfy (37d). Let $i=0$.
repeat
  Calculate $\boldsymbol{\Lambda}_1$, $\boldsymbol{c}_1$, d_1, $\boldsymbol{\Lambda}_2$, $\boldsymbol{c}_2$, and d_2.
  Solve (37a), (37b) and (37c) by CVX and obtain $\boldsymbol{v}$.
  if $\boldsymbol{v}$ satisfies (37d) **then**
    Let $i=i+1$ and $\boldsymbol{V}^{(i)}=[v_1,\ldots v_M;v_{M+1},\ldots v_{2M}]$.
  end if
until convergence
Let $\boldsymbol{V}^{(i)}$ be the solution of problem (29).

F. Updating Receive Antenna Positions

In the following, we address the sub-problem of optimizing $\boldsymbol{U}$ using the proposed lemmas and the SCA algorithm. With fixed $\{\boldsymbol{V},\boldsymbol{w}_{\mathrm{t}},\boldsymbol{w}_{\mathrm{r}},p_{\mathrm{u}},\boldsymbol{\Delta},\boldsymbol{\omega}\}$, (22) can be recast as

$$\begin{aligned}\max_{\boldsymbol{U}}\ & 2\mathrm{Re}\{\omega_{\mathrm{u}}^H\boldsymbol{w}_{\mathrm{r}}^H\boldsymbol{h}_{\mathrm{u}}(\boldsymbol{U})\}-|\omega_{\mathrm{u}}|^2\Big(p_{\mathrm{u}}\left|\boldsymbol{w}_{\mathrm{r}}^H\boldsymbol{h}_{\mathrm{u}}(\boldsymbol{U})\right|^2+\left|\boldsymbol{w}_{\mathrm{r}}^H\boldsymbol{H}(\boldsymbol{U})\boldsymbol{w}_{\mathrm{t}}\right|^2\Big)\\ \text{s.t.}\ & \left|\boldsymbol{w}_{\mathrm{r}}^H\boldsymbol{H}_{\mathrm{s}}(\boldsymbol{U})\boldsymbol{w}_{\mathrm{t}}\right|^2-\eta p_{\mathrm{u}}\left|\boldsymbol{w}_{\mathrm{r}}^H\boldsymbol{h}_{\mathrm{u}}(\boldsymbol{U})\right|^2-\eta\left|\boldsymbol{w}_{\mathrm{r}}^H\boldsymbol{H}_{\mathrm{SI}}(\boldsymbol{U})\boldsymbol{w}_{\mathrm{t}}\right|^2\geq\beta_2,\\ & \boldsymbol{u}_n,\boldsymbol{u}_{n'}\in\mathcal{S},\boldsymbol{u}_n\neq\boldsymbol{u}_{n'},\ \forall n,n'\in\mathcal{N},n\neq n',\end{aligned} \tag{38}$$

where $\beta_2=\eta\sigma_{\mathrm{r}}^2\|\boldsymbol{w}_{\mathrm{r}}^H\|^2$. For convenience, denote $\boldsymbol{R}_{\mathrm{s}}(\boldsymbol{U})=\boldsymbol{a}_{\mathrm{r}}(\boldsymbol{U})$. Based on the model in Section II-B, (38) is

$$\begin{aligned}\max_{\boldsymbol{U}}\ & 2\mathrm{Re}\{\omega_{\mathrm{u}}^H\boldsymbol{w}_{\mathrm{r}}^H\boldsymbol{R}_{\mathrm{u}}(\boldsymbol{U})\boldsymbol{\Gamma}_{\mathrm{u}}\mathbf{1}\}-|\omega_{\mathrm{u}}|^2\Big(p_{\mathrm{u}}\left|\boldsymbol{w}_{\mathrm{r}}^H\boldsymbol{R}_{\mathrm{u}}(\boldsymbol{U})\boldsymbol{\Gamma}_{\mathrm{u}}\mathbf{1}\right|^2\\ & +\left|\alpha_{\mathrm{s}}\boldsymbol{w}_{\mathrm{r}}^H\boldsymbol{R}_{\mathrm{s}}(\boldsymbol{U})\boldsymbol{a}_{\mathrm{t}}^H\boldsymbol{w}_{\mathrm{t}}\right|^2+\left|\boldsymbol{w}_{\mathrm{r}}^H\boldsymbol{R}_{\mathrm{SI}}(\boldsymbol{U})\boldsymbol{\Gamma}_{\mathrm{SI}}\boldsymbol{T}_{\mathrm{SI}}^H\boldsymbol{w}_{\mathrm{t}}\right|^2\\ & +2\mathrm{Re}\{\left(\alpha_{\mathrm{s}}\boldsymbol{w}_{\mathrm{r}}^H\boldsymbol{R}_{\mathrm{s}}(\boldsymbol{U})\boldsymbol{a}_{\mathrm{t}}^H\boldsymbol{w}_{\mathrm{t}}\right)\left(\boldsymbol{w}_{\mathrm{r}}^H\boldsymbol{R}_{\mathrm{SI}}(\boldsymbol{U})\boldsymbol{\Gamma}_{\mathrm{SI}}\boldsymbol{T}_{\mathrm{SI}}^H\boldsymbol{w}_{\mathrm{t}}\right)^H\}\Big)\\ \text{s.t.}\ & \Big(\eta p_{\mathrm{u}}\left|\boldsymbol{w}_{\mathrm{r}}^H\boldsymbol{R}_{\mathrm{u}}(\boldsymbol{U})\boldsymbol{\Gamma}_{\mathrm{u}}\mathbf{1}\right|^2+\eta\left|\boldsymbol{w}_{\mathrm{r}}^H\boldsymbol{R}_{\mathrm{SI}}(\boldsymbol{U})\boldsymbol{\Gamma}_{\mathrm{SI}}\boldsymbol{T}_{\mathrm{SI}}^H\boldsymbol{w}_{\mathrm{t}}\right|^2\\ & -\left|\alpha_{\mathrm{s}}\boldsymbol{w}_{\mathrm{r}}^H\boldsymbol{R}_{\mathrm{s}}(\boldsymbol{U})\boldsymbol{a}_{\mathrm{t}}^H\boldsymbol{w}_{\mathrm{t}}\right|^2+\beta_2\Big)\leq0,\\ & \boldsymbol{u}_n,\boldsymbol{u}_{n'}\in\mathcal{S},\boldsymbol{u}_n\neq\boldsymbol{u}_{n'},\ \forall n,n'\in\mathcal{N},n\neq n'.\end{aligned} \tag{39}$$

Although (39) cannot be transformed directly into a convex problem, we can obtain the concave and convex quadratic surrogate functions for the terms in (39) based on Theorems 1–3. For convenience, we denote $\boldsymbol{u}=\mathrm{vector}\{\boldsymbol{U}\}=[x_1^{\mathrm{r}},\ldots,x_N^{\mathrm{r}},y_1^{\mathrm{r}},\ldots,y_N^{\mathrm{r}}]^T=[u_1,\ldots,u_{2N}]^T$.

Lemma 1. *For $\chi_2\in\{\mathrm{u},\mathrm{SI},\mathrm{s}\}$, $\forall\boldsymbol{a}=[a_1,\ldots,a_L]^T$ and $\forall\boldsymbol{b}=[b_1,\ldots,b_N]^T$, we can construct concave and convex quadratic surrogate functions for $|\boldsymbol{b}^T\boldsymbol{R}_{\chi_2}(\boldsymbol{U})\boldsymbol{a}|^2$ as $\boldsymbol{u}^T\hat{\boldsymbol{\Omega}}\boldsymbol{u}+\hat{\boldsymbol{p}}\boldsymbol{u}+\hat{q}$ and $-\boldsymbol{u}^T\bar{\boldsymbol{\Omega}}\boldsymbol{u}+\bar{\boldsymbol{p}}\boldsymbol{v}+\bar{q}$, respectively, according to the transformation in (40) and Theorem 1.*

Proof: Now we omit the subscript χ_2 for brevity. For vectors $\boldsymbol{a}=[a_1,\ldots,a_L]^T$ and $\boldsymbol{b}=[b_1,\ldots,b_N]^T$, we know that $\boldsymbol{b}^T\boldsymbol{R}(\boldsymbol{U})\boldsymbol{a}=\sum_{l=1}^{L}\sum_{n=1}^{N}a_l r_l(\boldsymbol{u}_n)b_n$, where $r_l(\boldsymbol{u}_n)=$

$e^{-j\frac{2\pi}{\lambda}\rho_l(\boldsymbol{u}_n)}$. Then, similar to (49), $|\boldsymbol{b}^T\boldsymbol{R}(\boldsymbol{U})\boldsymbol{a}|^2$ becomes

$$\begin{aligned}&|\boldsymbol{b}^T\boldsymbol{R}(\boldsymbol{U})\boldsymbol{a}|^2\\&=\sum_{i=1}^{L}\sum_{m=1}^{N}\sum_{l=1}^{L}\sum_{n=1}^{N}a_l r_l(\boldsymbol{u}_n)b_n b_m^H r_i^H(\boldsymbol{u}_m)a_i^H\\&=\sum_{i=1}^{L}\sum_{l=1}^{L}|a_i||a_l|\left[\sum_{m=1}^{N}\sum_{n=1}^{N}|b_m||b_n|\cos\left(\hat{f}_{i,l}(\boldsymbol{u}_m,\boldsymbol{u}_n)\right)\right],\end{aligned}\tag{40}$$

where $\hat{f}_{i,l}(\boldsymbol{u}_m,\boldsymbol{u}_n)=\frac{2\pi}{\lambda}[\rho_i(\boldsymbol{u}_m)-\rho_l(\boldsymbol{u}_n)]+\angle(a_l b_n b_m^H a_i^H)$. Since (40) has a similar form to that of (49), the concave and convex quadratic surrogate functions of $|\boldsymbol{b}^T\boldsymbol{R}(\boldsymbol{U})\boldsymbol{a}|^2$ can be obtained using Theorem 1 by taking $\hat{f}_{i,l}\to f_{i,l}$, $\boldsymbol{u}\to\boldsymbol{v}$, and $N\to M$. As a consequence, Lemma 1 is now proven. ■

Using Lemma 1, we can derive a concave quadratic surrogate functions of $\left|\alpha_{\mathrm{s}}\boldsymbol{w}_{\mathrm{r}}^H\boldsymbol{R}_{\mathrm{s}}(\boldsymbol{U})\boldsymbol{a}_{\mathrm{t}}^H\boldsymbol{w}_{\mathrm{t}}\right|^2$ as

$$\boldsymbol{u}^T\hat{\boldsymbol{\Omega}}_{\mathrm{s}}\boldsymbol{u}+\hat{\boldsymbol{p}}_{\mathrm{s}}\boldsymbol{u}+\hat{q}_{\mathrm{s}},\tag{41}$$

and furthermore, the convex quadratic surrogate functions of $\left|\boldsymbol{w}_{\mathrm{r}}^H\boldsymbol{R}_{\mathrm{u}}(\boldsymbol{U})\boldsymbol{\Gamma}_{\mathrm{u}}\mathbf{1}\right|^2$, $\left|\alpha_{\mathrm{s}}\boldsymbol{w}_{\mathrm{r}}^H\boldsymbol{R}_{\mathrm{s}}(\boldsymbol{U})\boldsymbol{a}_{\mathrm{t}}^H\boldsymbol{w}_{\mathrm{t}}\right|^2$, and $\left|\boldsymbol{w}_{\mathrm{r}}^H\boldsymbol{R}_{\mathrm{SI}}(\boldsymbol{U})\boldsymbol{\Gamma}_{\mathrm{SI}}\boldsymbol{T}_{\mathrm{SI}}^H\boldsymbol{w}_{\mathrm{t}}\right|^2$ are obtained as

$$-\boldsymbol{u}^T\hat{\boldsymbol{\Omega}}_{\mathrm{u}}\boldsymbol{u}+\bar{\boldsymbol{p}}_{\mathrm{u}}\boldsymbol{v}+\bar{q}_{\mathrm{u}},\tag{42}$$

$$-\boldsymbol{u}^T\hat{\boldsymbol{\Omega}}_{\mathrm{s}}\boldsymbol{u}+\bar{\boldsymbol{p}}_{\mathrm{s}}\boldsymbol{v}+\bar{q}_{\mathrm{s}},\tag{43}$$

$$-\boldsymbol{u}^T\hat{\boldsymbol{\Omega}}_{\mathrm{SI}}\boldsymbol{u}+\bar{\boldsymbol{p}}_{\mathrm{SI}}\boldsymbol{v}+\bar{q}_{\mathrm{SI}}.\tag{44}$$

Lemma 2. *For any vectors $\boldsymbol{a}=[a_1,\ldots,a_L]^T$ and $\boldsymbol{b}=[b_1,\ldots,b_N]^T$, $\boldsymbol{u}^T\tilde{\boldsymbol{\Omega}}\boldsymbol{u}+\tilde{\boldsymbol{p}}\boldsymbol{u}+\tilde{q}$ is a concave quadratic surrogate function for $\mathrm{Re}\{\boldsymbol{b}^T\boldsymbol{R}_{\chi_2}(\boldsymbol{U})\boldsymbol{a}\}$ $\forall\chi_2\in\{\mathrm{u},\mathrm{SI},\mathrm{s}\}$, where $\tilde{\boldsymbol{\Omega}}$ is NSD, and $\tilde{\boldsymbol{\Omega}}$, $\tilde{\boldsymbol{p}}$ and $\tilde{q}$ are given in (66).*

Proof: See Appendix D. ■

Based on Lemma 2, a concave quadratic surrogate function of $\mathrm{Re}\{\omega_{\mathrm{u}}^H\boldsymbol{w}_{\mathrm{r}}^H\boldsymbol{R}_{\mathrm{u}}(\boldsymbol{U})\boldsymbol{\Gamma}_{\mathrm{u}}\mathbf{1}\}$ can be obtained as

$$\boldsymbol{u}^T\tilde{\boldsymbol{\Omega}}_{\mathrm{u}}\boldsymbol{u}+\tilde{\boldsymbol{p}}_{\mathrm{u}}\boldsymbol{u}+\tilde{q}_{\mathrm{u}}.\tag{45}$$

Lemma 3. *By letting $\check{f}'_{i,l}\to\check{f}_{i,l}$, $\boldsymbol{u}\to\boldsymbol{v}$, and $N\to M$, a convex quadratic surrogate function of $\mathrm{Re}\{\left(\boldsymbol{b}^T\boldsymbol{R}_{\check{\chi}}(\boldsymbol{U})\check{\boldsymbol{a}}\right)\left(\boldsymbol{b}^T\boldsymbol{R}_{\chi}(\boldsymbol{U})\boldsymbol{a}\right)^H\}$ can be written as $\boldsymbol{u}^T\check{\boldsymbol{\Omega}}\boldsymbol{u}+\check{\boldsymbol{p}}\boldsymbol{u}+\check{q}$ using Theorem 3, where $\chi,\check{\chi}\in\{\mathrm{u},\mathrm{SI},\mathrm{s}\},\chi\neq\check{\chi}$, $\boldsymbol{a}\in\mathbb{C}^{L\times1}$, $\check{\boldsymbol{a}}\in\mathbb{C}^{\check{L}\times1}$ and $\boldsymbol{b}\in\mathbb{C}^{N\times1}$.*

Proof: With $\boldsymbol{a}=[a_1,\ldots,a_L]^T$, $\boldsymbol{b}=[b_1,\ldots,b_N]^T$, and $\check{\boldsymbol{a}}=[\check{a}_1,\ldots,\check{a}_{\check{L}}]^T$, we get $\boldsymbol{b}^T\boldsymbol{R}_{\chi}(\boldsymbol{U})\boldsymbol{a}=\sum_{i=1}^{L}\sum_{m=1}^{N}a_i r_i^{\chi}(\boldsymbol{u}_m)b_m$ and $\boldsymbol{b}^T\boldsymbol{R}_{\check{\chi}}(\boldsymbol{U})\check{\boldsymbol{a}}=\sum_{l=1}^{\check{L}}\sum_{n=1}^{N}\check{a}_l r_l^{\check{\chi}}(\boldsymbol{u}_n)b_n$, where $r_i^{\chi}(\boldsymbol{u}_m)=e^{-j\frac{2\pi}{\lambda}\rho_i^{\chi}(\boldsymbol{u}_m)}$. Then, similar to (60), we obtain

$$\begin{aligned}&\mathrm{Re}\left\{\left(\boldsymbol{b}^T\boldsymbol{R}_{\check{\chi}}(\boldsymbol{U})\check{\boldsymbol{a}}\right)\left(\boldsymbol{b}^T\boldsymbol{R}_{\chi}(\boldsymbol{U})\boldsymbol{a}\right)^H\right\}\\&=\mathrm{Re}\left\{\sum_{i=1}^{L}\sum_{m=1}^{N}\sum_{l=1}^{\check{L}}\sum_{n=1}^{N}\check{a}_l r_l^{\check{\chi}}(\boldsymbol{u}_n)b_n b_m^H(r_i^{\chi}(\boldsymbol{u}_m))^H a_i^H\right\}\\&=\sum_{i=1}^{L}\sum_{l=1}^{\check{L}}|a_i||\check{a}_l|\left[\sum_{m=1}^{N}\sum_{n=1}^{N}|b_m||b_n|\cos\left(\check{f}'_{i,l}(\boldsymbol{u}_m,\boldsymbol{u}_n)\right)\right],\end{aligned}\tag{46}$$

where $\check{f}'_{i,l}(\boldsymbol{u}_m,\boldsymbol{u}_n)=\frac{2\pi}{\lambda}[\rho_i^{\chi}(\boldsymbol{u}_m)-\rho_l^{\check{\chi}}(\boldsymbol{u}_n)]+\angle(\check{a}_l b_n b_m^H a_i^H)$. Considering $\check{f}'_{i,l}\to\check{f}_{i,l}$, $\boldsymbol{u}\to\boldsymbol{v}$, and $N\to M$, (46) is the same as (60). The convex surrogate function $\boldsymbol{u}^T\check{\boldsymbol{\Omega}}\boldsymbol{u}+\check{\boldsymbol{p}}\boldsymbol{u}+\check{q}$ can thus be obtained by Theorem 3, which proves Lemma 3. ■

Based on Lemma 3, we can now express the convex quadratic surrogate function for $\mathrm{Re}\{\left(\alpha_{\mathrm{s}}\boldsymbol{w}_{\mathrm{r}}^H\boldsymbol{R}_{\mathrm{s}}(\boldsymbol{U})\boldsymbol{a}_{\mathrm{t}}^H\boldsymbol{w}_{\mathrm{t}}\right)\left(\boldsymbol{w}_{\mathrm{r}}^H\boldsymbol{R}_{\mathrm{SI}}(\boldsymbol{U})\boldsymbol{\Gamma}_{\mathrm{SI}}\boldsymbol{T}_{\mathrm{SI}}^H\boldsymbol{w}_{\mathrm{t}}\right)^H\}$ as

$$\boldsymbol{v}^T\check{\boldsymbol{\Omega}}_{\mathrm{sSI}}\boldsymbol{v}+\check{\boldsymbol{p}}_{\mathrm{sSI}}\boldsymbol{v}+\check{q}_{\mathrm{sSI}}.\tag{47}$$

Denoting $\boldsymbol{\Omega}_1=2\tilde{\boldsymbol{\Omega}}_{\mathrm{u}}+|\omega_{\mathrm{u}}|^2(p_{\mathrm{u}}\hat{\boldsymbol{\Omega}}_{\mathrm{u}}+\hat{\boldsymbol{\Omega}}_{\mathrm{s}}+\hat{\boldsymbol{\Omega}}_{\mathrm{SI}}-2\check{\boldsymbol{\Omega}}_{\mathrm{sSI}})$, $\boldsymbol{p}_1=2\tilde{\boldsymbol{p}}_{\mathrm{u}}-|\omega_{\mathrm{u}}|^2(p_{\mathrm{u}}\bar{\boldsymbol{p}}_{\mathrm{u}}+\bar{\boldsymbol{p}}_{\mathrm{s}}+\bar{\boldsymbol{p}}_{\mathrm{SI}}+2\check{\boldsymbol{p}}_{\mathrm{sSI}})$, $q_1=2\tilde{q}_{\mathrm{u}}-|\omega_{\mathrm{u}}|^2(p_{\mathrm{u}}\bar{q}_{\mathrm{u}}+\bar{q}_{\mathrm{s}}+\bar{q}_{\mathrm{SI}}+2\check{q}_{\mathrm{sSI}})$, $\boldsymbol{\Omega}_2=-\eta p_{\mathrm{u}}\hat{\boldsymbol{\Omega}}_{\mathrm{u}}-\eta\hat{\boldsymbol{\Omega}}_{\mathrm{SI}}-\hat{\boldsymbol{\Omega}}_{\mathrm{s}}$, $\boldsymbol{p}_2=\eta p_{\mathrm{u}}\bar{\boldsymbol{p}}_{\mathrm{u}}+\eta\bar{\boldsymbol{p}}_{\mathrm{SI}}-\hat{\boldsymbol{p}}_{\mathrm{s}}$, and $q_2=\eta p_{\mathrm{u}}\bar{q}_{\mathrm{u}}+\eta\bar{q}_{\mathrm{SI}}-\hat{q}_{\mathrm{s}}$, (39) is transformed to

$$\max_{\boldsymbol{u}}\quad\boldsymbol{u}^T\boldsymbol{\Omega}_1\boldsymbol{u}+\boldsymbol{p}_1\boldsymbol{u}+q_1,\tag{48a}$$

$$\text{s.t.}\quad\boldsymbol{u}^T\boldsymbol{\Omega}_2\boldsymbol{u}+\boldsymbol{p}_2\boldsymbol{u}+q_2\leq-\beta_2,\tag{48b}$$

$$0\leq u_n\leq W,n=1,\ldots,2N,\tag{48c}$$

$$[u_n,u_{n+N}]\neq[u_{n'},u_{n'+N}],\ \forall n,n'\in\mathcal{N},n\neq n'.\tag{48d}$$

Note that (48) has the same form as (37). Therefore, we can solve the original problem (38) using Algorithm 1.

G. Alternative Optimization

So far, we have provided different schemes for optimizing each variable. Overall, the main steps of solving problem (16) can be summarized in Algorithm 2. The summary of the proposed theorems and lemmas is given in Table I.

Algorithm 2 Alternative optimization for solving (16)

Initialize: $\boldsymbol{w}_{\mathrm{t}},\boldsymbol{w}_{\mathrm{r}},p_{\mathrm{u}},\boldsymbol{V},\boldsymbol{U}$.

Using the FP framework to reformulate the original problem (16) as (22) by introducing variables $\boldsymbol{\Delta}$ and $\boldsymbol{\omega}$.

repeat

1. *Update $\boldsymbol{\Delta}$ and $\boldsymbol{\omega}$* using (18) and (21), respectively.
2. *Optimize $\boldsymbol{w}_t$:* obtain the sub-problem (23) of optimizing the transmit beamforming vector and update $\boldsymbol{w}_{\mathrm{t}}$ via (25).
3. *Optimize $\boldsymbol{w}_r$:* solve the sub-problem (26) using CVX to optimize the receive beamforming vector $\boldsymbol{w}_{\mathrm{t}}$.
4. *Optimize p_u:* obtain the sub-problem (27) of optimizing the uplink transmit power p_{u} and optimize it through the closed-form solution in (28), respectively.
5. *Optimize $\boldsymbol{V}$:* transform the sub-problem (29) into (37) based on Theorems 1, 2, 3 and update the transmit FAS positions $\boldsymbol{V}$ by using Algorithm 1.
6. *Optimize $\boldsymbol{U}$:* transform the sub-problem (38) into (48) based on Lemmas 1, 2, 3 and update the receive FAS positions $\boldsymbol{U}$ by using Algorithm 1.

until convergence

H. Convergence and Complexity Analysis

1) Convergence Analysis: To begin, we denote the objective function of (29) by $f(\boldsymbol{v})$ and (37a) by $g(\boldsymbol{v})$. According to (53), (56), (59), and (63), we know that $f(\boldsymbol{v}^{(i+1)})\geq g(\boldsymbol{v}^{(i+1)}|\boldsymbol{v}^{(i)})$ and $f(\boldsymbol{v}^{(i)})=g(\boldsymbol{v}^{(i)}|\boldsymbol{v}^{(i)})$. In each iteration, we can always find $\boldsymbol{v}^{(i+1)}$ satisfying $g(\boldsymbol{v}^{(i+1)}|\boldsymbol{v}^{(i)})\geq g(\boldsymbol{v}^{(i)}|\boldsymbol{v}^{(i)})$.

The convergence of Algorithm 1 is thus guaranteed since $f(\boldsymbol{v}^{(i+1)}) \geq g(\boldsymbol{v}^{(i+1)}|\boldsymbol{v}^{(i)}) \geq g(\boldsymbol{v}^{(i)}|\boldsymbol{v}^{(i)}) = f(\boldsymbol{v}^{(i)})$.

For Algorithm 2, the communication rate increases in each iteration by optimizing $\boldsymbol{\Delta}, \boldsymbol{\omega}, \boldsymbol{w}_{\mathrm{t}}, \boldsymbol{w}_{\mathrm{r}}, p_{\mathrm{u}}, \boldsymbol{V}, \boldsymbol{U}$ iteratively. The convergence of Algorithm 2 is guaranteed since the communication rate is upper-bounded.

2) Complexity Analysis: We assume that the number of propagation paths for each channel is the same, i.e., $L_{\mathrm{d}} = L_{\mathrm{u}} = L_{\mathrm{SI}} = L$. Algorithm 1 involves solving a QCQP problem using CVX for a vector variable with $2M$ elements, which has a complexity of $\mathcal{O}((2M)^3)$. Denoting the maximum number of iterations in Algorithm 1 by N_{SCA}, the complexity of updating $\boldsymbol{V}$ and $\boldsymbol{U}$ using Algorithm 1 are $\mathcal{O}_{\boldsymbol{V}} = \mathcal{O}(N_{\mathrm{SCA}}[(2M)^3 + M^2L^2])$ and $\mathcal{O}_{\boldsymbol{U}} = \mathcal{O}(N_{\mathrm{SCA}}[(2N)^3 + N^2L^2])$, respectively. Calculating p_{u} based on (28) has a complexity of $\mathcal{O}_p = \mathcal{O}(NM)$. Denote the maximum number of iterations in optimizing $\boldsymbol{w}_{\mathrm{t}}$ and $\boldsymbol{w}_{\mathrm{r}}$ by N_{t} and N_{r}, respectively. The complexity of updating the beamforming vectors $\boldsymbol{w}_{\mathrm{t}}$ and $\boldsymbol{w}_{\mathrm{r}}$ are $\mathcal{O}_t = \mathcal{O}(N_t(M)^3 + M(N+M))$ and $\mathcal{O}_r = \mathcal{O}(N_r(N)^3 + N(N+M))$, respectively. Denote the maximum number of iterations of Algorithm 2 by N_{AO}, solving (16) requires a complexity of $\mathcal{O}(N_{\mathrm{AO}}(\mathcal{O}_t + \mathcal{O}_r + \mathcal{O}_p + \mathcal{O}_{\boldsymbol{V}} + \mathcal{O}_{\boldsymbol{U}}))$.

V. Simultion Results

Here, we evaluate the performance of the proposed algorithms using Monte Carlo simulation. The carrier frequency is 30 GHz. The azimuth and elevation AoAs and AoDs follow uniform distribution over $[0, \pi]$, and all the channel coefficients $\gamma \sim \mathcal{CN}(0,1)$. We assume that the number of paths is equal, i.e., $L_{\mathrm{d}} = L_{\mathrm{u}} = L_{\mathrm{SI}} = L$. Considering unit noise power, the maximum transmit signal-to-noise ratios (SNRs) of the BS and the uplink user are $\mathrm{SNR_t} = 10\log \mathrm{P_t}$ dB and $\mathrm{SNR_u} = 10\log \mathrm{P_u}$ dB. Unless otherwise specified, we set $W = 5\lambda$, $M = N = L = 2$, $\alpha_s = 10$, $\eta = 1$, $\mathrm{SNR_t} = 20$ dB, and $\mathrm{SNR_u} = 17$ dB in the simulations. We compare the proposed algorithm with the following benchmarks:

- **FPA-nonAO:** BS adopts FPAs with antenna spacing of $\lambda/2$, and the beamforming vectors and the transmit power are optimized once without iteration.
- **FPA-AO:** BS uses FPAs with antenna spacing of $\lambda/2$, and the beamforming vectors and the transmit power are alternatively optimized until convergence.
- **Transmit FAS (FAS-Tx):** The BS transmits signals using FAS while receiving signals using FPA. The positions of the transmit FAS $\boldsymbol{V}$ are optimized while the positions of FPA are fixed and spaced by $\lambda/2$.
- **Receive FAS (FAS-Rx):** The BS transmits signals using FPA while receiving signals using FAS. The positions of the receive FAS $\boldsymbol{U}$ are optimized while the positions of FPA are fixed and spaced by $\lambda/2$.
- **FAS-Tx+Rx:** The BS uses FAS for both transmitting and receiving signals.

In Fig. 2, we show the communication rate with different numbers of transmit BS antennas. As expected, the communication rate increases with M for all schemes. In particular, when M increases from 2 to 50, the communication rate obtained by using FAS increases by 3 bps/Hz. Note that FAS with 20 transmit antennas can outperform the FPA system with 50 transmit antennas when $N = 5$ and $N = 20$. While optimizing only the transmit FAS can significantly enhance the communication rate, updating both the transmit and receive FAS can further improve the communication performance.

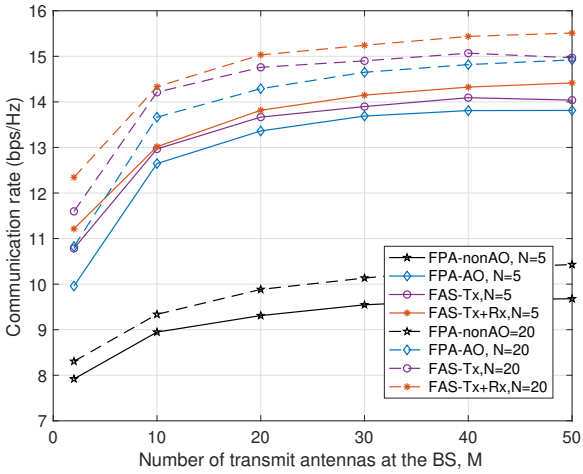

Fig. 2. Communication rate versus the number of transmit BS antennas, M.

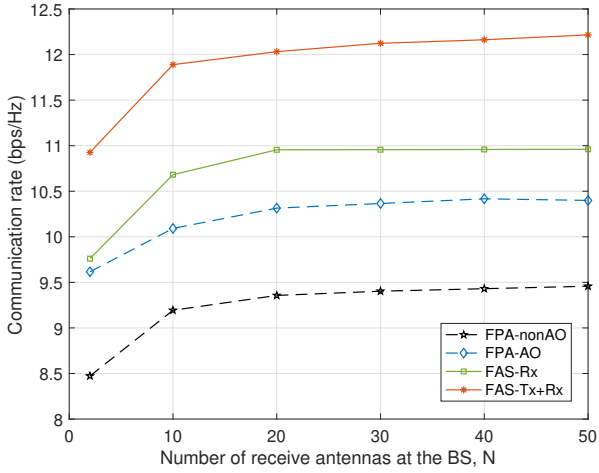

Fig. 3. Communication rate versus the number of receive BS antennas N.

Fig. 3 considers how the number of receive BS antennas affects the communication rate. By updating the positions of the receive antennas, the communication rate is increased by 1.5 bps/Hz compared to the FPA when $L = 2$. Optimizing both transmit and receive FAS also further increases the communication rate by 1.25 bps/Hz compared to optimizing only the receive FAS.

In Fig. 4, we verify the relationship between the communication rate and the number of paths. In comparison, updating the transmit FAS has better performance than updating the receive FAS. This is because both the uplink and downlink rates are related to the BS transmitter, but only the BS receiver is independent of the downlink rate. In addition, optimizing

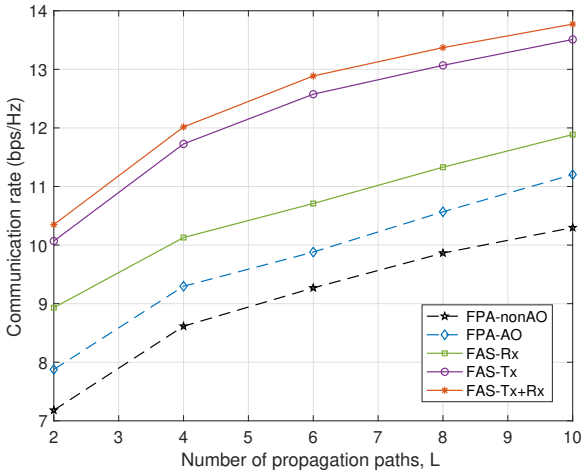

Fig. 4. Communication rate versus the number of propagation paths, L.

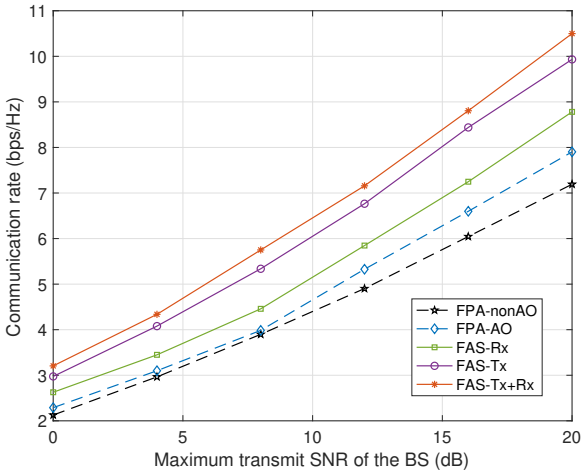

Fig. 6. Communication rate versus the maximum transmit SNR of the BS, $\mathrm{SNR_t} = 10\log \mathrm{P_t}$ dB.

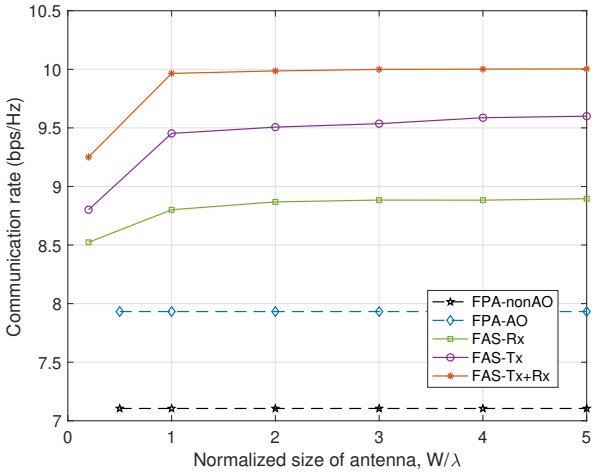

Fig. 5. Communication rate versus the normalized antenna size, W/λ.

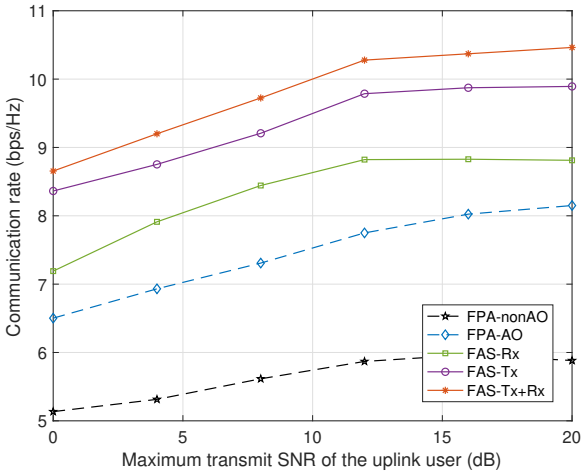

Fig. 7. Communication rate versus the maximum transmit SNR of the uplink user, $\mathrm{SNR_u} = 10\log \mathrm{P_u}$ dB.

both the transmit and receive FAS achieves the highest rate, showing an improvement of 2 bps/Hz over FPA.

In Fig. 5, we analyze how the communication rate changes with the size of FAS. We can see that the communication rate initially increases with the antenna size and then saturates. When the antenna size is small, the spatial DoF obtained by changing the antenna positions is limited, so is the performance. Once the antenna size is large enough, further increases in size no longer increase the communication performance.

Figs. 6 and 7 illustrate the communication rate obtained with different values of the power budgets of the BS and the uplink user, respectively. As expected, the communication rate increases with the power budgets. Compared to increasing the power budget of the uplink user, increasing the power budget of the BS contributes more to the communication rate since the downlink rate is independent of the uplink transmit power. As $\mathrm{SNR_t}$ increases from 0 dB to 20 dB, the communication rate obtained by using FAS and FPA increases by 7.5 bps/Hz and 5.8 bps/Hz, respectively. FAS always provides a 2 bps/Hz improvement compared to FPA as $\mathrm{SNR_u}$ increases.

Finally, in Fig. 8, we study the communication rate under different sensing thresholds. As we can see, the communication rate decreases for all schemes when the sensing threshold increases. As η increases, the communication rate obtained by FAS shows more decrease compared to FPA. However, when $\eta = 5$, FAS still outperforms FPA by more than 1 bps/Hz.

VI. Conclusion

This paper addressed the problem of maximizing the communication rate under sensing performance and power budget constraints. We first introduced the FP framework to transform the problem into subproblems, each of which could be solved in an iterative manner. In particular, the beamforming vectors were optimized using the MM algorithm, while a closed-form solution of the uplink transmit power was given. In addition,

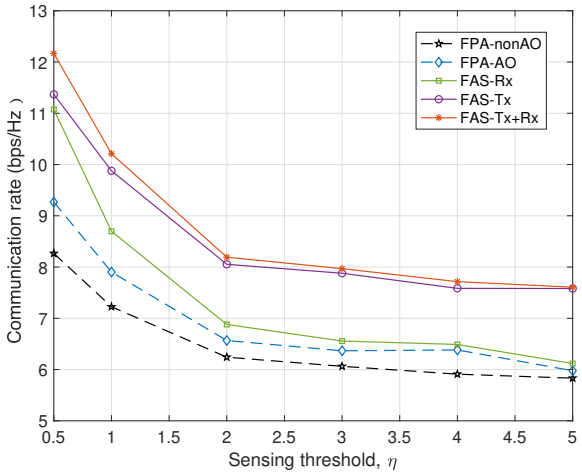

Fig. 8. Communication rate versus the sensing threshold, η.

we provided an SCA-based algorithm to optimize the antenna positions by transforming the corresponding subproblems into convex forms. Simulation results demonstrated that using the proposed algorithm, FAS greatly outperforms FPA in terms of communication rate for ISAC tasks. It is noted that in real-time systems, hardware constraints such as processing latency, response times, and energy consumption should be carefully taken into account. As such, future research should consider these practical limitations and explore the development of low-complexity, real-time-compatible algorithms to enable efficient deployment of FAS in real-world scenarios.

Appendix A
Proof of Theorem 1

Subscript χ_1 is omitted in this proof for notational brevity. For vectors $\boldsymbol{a} = [a_1, \ldots, a_L]^T$ and $\boldsymbol{b} = [b_1, \ldots, b_M]^T$, we have $\boldsymbol{a}^T\boldsymbol{T}^H(\boldsymbol{V})\boldsymbol{b} = \sum_{i=1}^{L}\sum_{m=1}^{M} a_i t_i^H(\boldsymbol{v}_m) b_m$, where $t_i(\boldsymbol{v}_m) = e^{-j\frac{2\pi}{\lambda}\rho_i(\boldsymbol{v}_m)}$. Then we have

$$
\begin{aligned}
|\boldsymbol{a}^T\boldsymbol{T}(\boldsymbol{V})^H\boldsymbol{b}|^2 &= \sum_{i=1}^{L}\sum_{m=1}^{M}\sum_{l=1}^{L}\sum_{n=1}^{M} a_i t_i^H(\boldsymbol{v}_m) b_m b_n^H t_l(\boldsymbol{v}_n) a_l^H \\
&= \sum_{i=1}^{L}\sum_{m=1}^{M}\sum_{l=1}^{L}\sum_{n=1}^{M} a_i b_m b_n^H a_l^H e^{j\frac{2\pi}{\lambda}[\rho_i(\boldsymbol{v}_m)-\rho_l(\boldsymbol{v}_n)]} \\
&\overset{(a)}{=} \sum_{i=1}^{L}\sum_{m=1}^{M}\sum_{l=1}^{L}\sum_{n=1}^{M} \mathrm{Re}\left\{ a_i b_m b_n^H a_l^H e^{j\frac{2\pi}{\lambda}[\rho_i(\boldsymbol{v}_m)-\rho_l(\boldsymbol{v}_n)]} \right\} \\
&= \sum_{i=1}^{L}\sum_{m=1}^{M}\sum_{l=1}^{L}\sum_{n=1}^{M} |a_i b_m b_n^H a_l^H| \cos\left(f_{i,l}(\boldsymbol{v}_m, \boldsymbol{v}_n)\right) \\
&\overset{(b)}{=} \sum_{i=1}^{L}\sum_{m=1}^{M}\sum_{l=1}^{L}\sum_{n=1}^{M} |a_i||b_m||b_n||a_l| \cos\left(f_{i,l}(\boldsymbol{v}_m, \boldsymbol{v}_n)\right) \\
&= \sum_{i=1}^{L}\sum_{l=1}^{L} |a_i||a_l| \left[\sum_{m=1}^{M}\sum_{n=1}^{M} |b_m||b_n| \cos\left(f_{i,l}(\boldsymbol{v}_m, \boldsymbol{v}_n)\right) \right],
\end{aligned} \tag{49}
$$

where $f_{i,l}(\boldsymbol{v}_m, \boldsymbol{v}_n) = \frac{2\pi}{\lambda}[\rho_i(\boldsymbol{v}_m) - \rho_l(\boldsymbol{v}_n)] + \angle(a_i b_m b_n^H a_l^H)$, equation (a) holds since $|\boldsymbol{a}^T\boldsymbol{T}(\boldsymbol{V})^H\boldsymbol{b}|^2$ is real, and equation (b) holds due to the fact that $|pq| = |p||q|\ \forall p, q \in \mathbb{C}$. Based on Taylor series expansion, we can construct a concave quadratic surrogate function g for any cosine function as

$$
\begin{aligned}
\cos(\psi) &\overset{(c)}{\approx} \cos(\psi_0) - \sin(\psi_0)(\psi - \psi_0) - \frac{1}{2}\cos(\psi_0)(\psi - \psi_0)^2 \\
&\overset{(d)}{\geq} g(\psi|\psi_0) \triangleq \cos(\psi_0) - \sin(\psi_0)(\psi - \psi_0) - \frac{1}{2}(\psi - \psi_0)^2,
\end{aligned} \tag{50}
$$

where (c) is the second order Taylor series expansion of the cosine function, and (d) holds since $\cos(\psi_0) \leq 1$. Denoting $\boldsymbol{v}_{m,0}$ and $\boldsymbol{v}_{n,0}$ as the position vectors obtained in the previous iteration and using (50), we know that

$$
\begin{aligned}
&\cos(f_{i,l}(\boldsymbol{v}_m, \boldsymbol{v}_n)) \geq g(f_{i,l}(\boldsymbol{v}_m, \boldsymbol{v}_n)|f_{i,l}(\boldsymbol{v}_{m,0}, \boldsymbol{v}_{n,0})) \\
&= \cos\left(f_{i,l,m,n}^0\right) - \sin\left(f_{i,l,m,n}^0\right)\left(f_{i,l}(\boldsymbol{v}_m, \boldsymbol{v}_n) - f_{i,l,m,n}^0\right) \\
&\quad - \frac{1}{2}(f_{i,l}(\boldsymbol{v}_m, \boldsymbol{v}_n) - f_{i,l,m,n}^0)^2 \\
&= \cos\left(f_{i,l,m,n}^0\right) - \sin\left(f_{i,l,m,n}^0\right)\left(\frac{2\pi}{\lambda}[\rho_i(\boldsymbol{v}_m) - \rho_l(\boldsymbol{v}_n)] - \tau_{i,l,m,n}\right) \\
&\quad - \frac{1}{2}\left(\frac{2\pi}{\lambda}[\rho_i(\boldsymbol{v}_m) - \rho_l(\boldsymbol{v}_n)] - \tau_{i,l,m,n}\right)^2 \\
&= \cos\left(f_{i,l,m,n}^0\right) - \sin\left(f_{i,l,m,n}^0\right)\left(\frac{2\pi}{\lambda} z_{i,l}(\boldsymbol{v}_m, \boldsymbol{v}_n) - \tau_{i,l,m,n}\right) \\
&\quad - \frac{1}{2}\left(\frac{2\pi}{\lambda} z_{i,l}(\boldsymbol{v}_m, \boldsymbol{v}_n) - \tau_{i,l,m,n}\right)^2 \\
&= \frac{-2\pi^2}{\lambda^2}\left(z_{i,l}(\boldsymbol{v}_m, \boldsymbol{v}_n)\right)^2 + \frac{2\pi}{\lambda}\left(\tau_{i,l,m,n} - \sin(f_{i,l,m,n}^0)\right) z_{i,l}(\boldsymbol{v}_m, \boldsymbol{v}_n) \\
&\quad + \cos\left(f_{i,l,m,n}^0\right) + \sin\left(f_{i,l,m,n}^0\right)\tau_{i,l,m,n} - \frac{1}{2}\tau_{i,l,m,n}^2,
\end{aligned} \tag{51}
$$

where $f_{i,l,m,n}^0 = f_{i,l}(\boldsymbol{v}_{m,0}, \boldsymbol{v}_{n,0})$, $\tau_{i,l,m,n} = \frac{2\pi}{\lambda}[\rho_i(\boldsymbol{v}_{m,0}) - \rho_l(\boldsymbol{v}_{n,0})]$, and $z_{i,l}(\boldsymbol{v}_m, \boldsymbol{v}_n) = \rho_i(\boldsymbol{v}_m) - \rho_l(\boldsymbol{v}_n) = x_m^{\mathrm{t}}\delta_i + y_m^{\mathrm{t}}\xi_i - x_n^{\mathrm{t}}\delta_l - y_n^{\mathrm{t}}\xi_l$. Then we obtain a lower-bound of (49) as

$$
\begin{aligned}
&|\boldsymbol{a}^T\boldsymbol{T}(\boldsymbol{V})^H\boldsymbol{b}|^2 \\
&\geq \sum_{i=1}^{L}\sum_{l=1}^{L} |a_i||a_l| \left[\sum_{m=1}^{M}\sum_{n=1}^{M} |b_m||b_n| g\left(f_{i,l}(\boldsymbol{v}_m, \boldsymbol{v}_n)|f_{i,l}(\boldsymbol{v}_{m,0}, \boldsymbol{v}_{n,0})\right) \right] \\
&= \sum_{i=1}^{L}\sum_{l=1}^{L} |a_i||a_l| \left[\boldsymbol{v}^T\hat{\boldsymbol{A}}_{i,l}\boldsymbol{v} + \hat{\boldsymbol{c}}_{i,l}\boldsymbol{v} + \hat{d}_{i,l} \right],
\end{aligned} \tag{52}
$$

where

$$\hat{\boldsymbol{\Lambda}}_{i,l} = \frac{-2\pi^2}{\lambda^2}\begin{bmatrix}\boldsymbol{A}_{i,l} & \boldsymbol{C}_{i,l}\\ \boldsymbol{C}_{i,l} & \boldsymbol{B}_{i,l}\end{bmatrix},$$
$$\boldsymbol{A}_{i,l} = (\delta_i^2+\delta_l^2)\mathrm{diag}(\kappa\bar{\boldsymbol{b}}) - 2\delta_i\delta_l\bar{\boldsymbol{b}}\bar{\boldsymbol{b}}^T,$$
$$\boldsymbol{B}_{i,l} = (\xi_i^2+\xi_l^2)\mathrm{diag}(\kappa\bar{\boldsymbol{b}}) - 2\xi_i\xi_l\bar{\boldsymbol{b}}\bar{\boldsymbol{b}}^T,$$
$$\boldsymbol{C}_{i,l} = (\delta_i\xi_i+\delta_l\xi_l)\mathrm{diag}(\kappa\bar{\boldsymbol{b}}) - (\delta_i\xi_l+\delta_l\xi_i)\bar{\boldsymbol{b}}\bar{\boldsymbol{b}}^T,$$
$$\bar{\boldsymbol{b}} = [|b_1|,\ldots,|b_M|]^T,$$
$$\kappa = \sum_{m=1}^{M}|b_m|,$$
$$\hat{\boldsymbol{c}}_{i,l} = \frac{2\pi}{\lambda}[\delta_i\boldsymbol{\Upsilon}_{i,l} - \delta_l\boldsymbol{\Psi}_{i,l}, \xi_i\boldsymbol{\Upsilon}_{i,l} - \xi_l\boldsymbol{\Psi}_{i,l}],$$
$$\boldsymbol{\Upsilon}_{i,l} = [|b_1|\Upsilon_1^{i,l},\ldots,|b_M|\Upsilon_M^{i,l}],$$
$$\boldsymbol{\Psi}_{i,l} = [|b_1|\Psi_1^{i,l},\ldots,|b_M|\Psi_M^{i,l}],$$
$$\Upsilon_m^{i,l} = \sum_{n=1}^{M}|b_n|\big(\tau_{i,l,m,n} - \sin(f^0_{i,l,m,n})\big),$$
$$\Psi_n^{i,l} = \sum_{m=1}^{M}|b_m|\big(\tau_{i,l,m,n} - \sin(f^0_{i,l,m,n})\big),$$
$$\hat{d}_{i,l} = \sum_{m=1}^{M}\sum_{n=1}^{M}|b_m||b_n|\hat{\varrho}_{i,l,m,n},$$
$$\hat{\varrho}_{i,l,m,n} \triangleq \cos\left(f^0_{i,l,m,n}\right) + \sin\left(f^0_{i,l,m,n}\right)\tau_{i,l,m,n} - \frac{1}{2}\tau^2_{i,l,m,n}.$$

Now, denoting $\hat{\boldsymbol{\Lambda}} = \sum_{i=1}^{L}\sum_{l=1}^{L}|a_i||a_l|\hat{\boldsymbol{\Lambda}}_{i,l}$, $\hat{\boldsymbol{c}} = \sum_{i=1}^{L}\sum_{l=1}^{L}|a_i||a_l|\hat{\boldsymbol{c}}_{i,l}$, and $\hat{d} = \sum_{i=1}^{L}\sum_{l=1}^{L}|a_i||a_l|\hat{d}_{i,l}$, (52) can be rewritten as

$$|\boldsymbol{a}^T\boldsymbol{T}(\boldsymbol{V})^H\boldsymbol{b}|^2 \geq \boldsymbol{v}^T\hat{\boldsymbol{\Lambda}}\boldsymbol{v} + \hat{\boldsymbol{c}}\boldsymbol{v} + \hat{d}. \tag{53}$$

Since $\hat{\boldsymbol{\Lambda}}_{i,l}$ is symmetric and $\boldsymbol{v}^T\hat{\boldsymbol{\Lambda}}_{i,l}\boldsymbol{v} = \frac{-2\pi^2}{\lambda^2}\sum_{m=1}^{M}\sum_{n=1}^{M}|b_m||b_n|\big(z_{i,l}(\boldsymbol{v}_m,\boldsymbol{v}_n)\big)^2 \leq 0$, $\hat{\boldsymbol{\Lambda}}_{i,l}$ is an NSD matrix, and so is $\hat{\boldsymbol{\Lambda}}$.

Similar to (50), a convex quadratic surrogate function $\bar{g}$ for the cos function can also be derived as

$$\cos(\psi) \approx \cos(\psi_0) - \sin(\psi_0)(\psi-\psi_0) - \frac{1}{2}\cos(\psi_0)(\psi-\psi_0)^2$$
$$\overset{(e)}{\leq} \bar{g}(\psi|\psi_0) \triangleq \cos(\psi_0) - \sin(\psi_0)(\psi-\psi_0) + \frac{1}{2}(\psi-\psi_0)^2, \tag{54}$$

where (e) holds due to $\cos(\psi_0) \geq -1$. Therefore, based on (54), we have

$$\begin{aligned}
&\cos(f_{i,l}(\boldsymbol{v}_m,\boldsymbol{v}_n)) \leq \bar{g}(f_{i,l}(\boldsymbol{v}_m,\boldsymbol{v}_n)|f_{i,l}(\boldsymbol{v}_{m,0},\boldsymbol{v}_{n,0}))\\
&= \cos\left(f^0_{i,l,m,n}\right) - \sin\left(f^0_{i,l,m,n}\right)\left(f_{i,l}(\boldsymbol{v}_m,\boldsymbol{v}_n) - f^0_{i,l,m,n}\right)\\
&\quad + \frac{1}{2}\left(f_{i,l}(\boldsymbol{v}_m,\boldsymbol{v}_n) - f^0_{i,l,m,n}\right)^2\\
&= \cos\left(f^0_{i,l,m,n}\right) - \sin\left(f^0_{i,l,m,n}\right)\left(\frac{2\pi}{\lambda}[\rho_i(\boldsymbol{v}_m) - \rho_l(\boldsymbol{v}_n)] - \tau_{i,l,m,n}\right)\\
&\quad + \frac{1}{2}\left(\frac{2\pi}{\lambda}[\rho_i(\boldsymbol{v}_m) - \rho_l(\boldsymbol{v}_n)] - \tau_{i,l,m,n}\right)^2\\
&= \cos\left(f^0_{i,l,m,n}\right) - \sin\left(f^0_{i,l,m,n}\right)\left(\frac{2\pi}{\lambda}z_{i,l}(\boldsymbol{v}_m,\boldsymbol{v}_n) - \tau_{i,l,m,n}\right)\\
&\quad + \frac{1}{2}\left(\frac{2\pi}{\lambda}z_{i,l}(\boldsymbol{v}_m,\boldsymbol{v}_n) - \tau_{i,l,m,n}\right)^2\\
&= \frac{2\pi^2}{\lambda^2}\big(z_{i,l}(\boldsymbol{v}_m,\boldsymbol{v}_n)\big)^2 - \frac{2\pi}{\lambda}\big(\tau_{i,l,m,n} + \sin(f^0_{i,l,m,n})\big)z_{i,l}(\boldsymbol{v}_m,\boldsymbol{v}_n)\\
&\quad + \cos\left(f^0_{i,l,m,n}\right) + \sin\left(f^0_{i,l,m,n}\right)\tau_{i,l,m,n} + \frac{1}{2}\tau^2_{i,l,m,n},
\end{aligned} \tag{55}$$

where $f^0_{i,l,m,n}$, $\tau_{i,l,m,n}$ and $z_{i,l}(\boldsymbol{v}_m,\boldsymbol{v}_n)$ are defined in (51). An upper-bound of (49) can thus be written as

$$\begin{aligned}
&|\boldsymbol{a}^T\boldsymbol{T}(\boldsymbol{V})^H\boldsymbol{b}|^2\\
&\leq \sum_{i=1}^{L}\sum_{l=1}^{L}|a_i||a_l|\left[\sum_{m=1}^{M}\sum_{n=1}^{M}|b_m||b_n|\bar{g}\big(f_{i,l}(\boldsymbol{v}_m,\boldsymbol{v}_n)|f_{i,l}(\boldsymbol{v}_{m,0},\boldsymbol{v}_{n,0})\big)\right]\\
&= \sum_{i=1}^{L}\sum_{l=1}^{L}|a_i||a_l|\left[-\boldsymbol{v}^T\hat{\boldsymbol{\Lambda}}_{i,l}\boldsymbol{v} + \bar{\boldsymbol{c}}_{i,l}\boldsymbol{v} + \bar{d}_{i,l}\right],\\
&= -\boldsymbol{v}^T\hat{\boldsymbol{\Lambda}}\boldsymbol{v} + \bar{\boldsymbol{c}}\boldsymbol{v} + \bar{d},
\end{aligned} \tag{56}$$

where $\hat{\boldsymbol{\Lambda}}_{i,l}$ is given in (52),

$$\bar{\boldsymbol{c}} = \sum_{i=1}^{L}\sum_{l=1}^{L}|a_i||a_l|\bar{\boldsymbol{c}}_{i,l},$$
$$\bar{d} = \sum_{i=1}^{L}\sum_{l=1}^{L}|a_i||a_l|\bar{d}_{i,l},$$
$$\bar{\boldsymbol{c}}_{i,l} = \frac{-2\pi}{\lambda}[\delta_i\bar{\boldsymbol{\Upsilon}}_{i,l} - \delta_l\bar{\boldsymbol{\Psi}}_{i,l}, \xi_i\bar{\boldsymbol{\Upsilon}}_{i,l} - \xi_l\bar{\boldsymbol{\Psi}}_{i,l}],$$
$$\bar{\boldsymbol{\Upsilon}}_{i,l} = [|b_1|\bar{\Upsilon}_1^{i,l},\ldots,|b_M|\bar{\Upsilon}_M^{i,l}],$$
$$\bar{\boldsymbol{\Psi}}_{i,l} = [|b_1|\bar{\Psi}_1^{i,l},\ldots,|b_M|\bar{\Psi}_M^{i,l}],$$
$$\bar{\Upsilon}_m^{i,l} = \sum_{n=1}^{M}|b_n|\big(\tau_{i,l,m,n} + \sin(f^0_{i,l,m,n})\big),$$
$$\bar{\Psi}_n^{i,l} = \sum_{m=1}^{M}|b_m|\big(\tau_{i,l,m,n} + \sin(f^0_{i,l,m,n})\big),$$
$$\bar{d}_{i,l} = \sum_{m=1}^{M}\sum_{n=1}^{M}|b_m||b_n|\bar{q}_{i,l,m,n},$$
$$\bar{q}_{i,l,m,n} = \cos\left(f^0_{i,l,m,n}\right) + \sin\left(f^0_{i,l,m,n}\right)\tau_{i,l,m,n} + \frac{1}{2}\tau^2_{i,l,m,n}.$$

Since $\hat{\boldsymbol{\Lambda}}$ is a NSD matrix as given in (53), $-\boldsymbol{v}^T\hat{\boldsymbol{\Lambda}}\boldsymbol{v} + \bar{\boldsymbol{c}}\boldsymbol{v} + \bar{d}$ is a convex quadratic function. This completes the proof.

Appendix B
Proof of Theorem 2

In the following, we omit the subscript χ_1 for brevity. Denote $\boldsymbol{a}=[a_1,\ldots,a_L]^T$ and $\boldsymbol{b}=[b_1,\ldots,b_M]^T$. Based on the transmitting steering matrices in Section II-B, we have

$$\begin{aligned}
&\mathrm{Re}\{\boldsymbol{a}^T\boldsymbol{T}(\boldsymbol{V})^H\boldsymbol{b}\}=\mathrm{Re}\left\{\sum_{i=1}^{L}\sum_{m=1}^{M}a_i t_i^H(\boldsymbol{v}_m)b_m\right\}\\
=&\mathrm{Re}\left\{\sum_{i=1}^{L}\sum_{m=1}^{M}a_i b_m e^{j\frac{2\pi}{\lambda}\rho_i(\boldsymbol{v}_m)}\right\}\\
=&\sum_{i=1}^{L}\sum_{m=1}^{M}|a_i b_m|\cos\left(\frac{2\pi}{\lambda}\rho_i(\boldsymbol{v}_m)+\angle a_i b_m\right)\\
\overset{\text{(f)}}{=}&\sum_{i=1}^{L}\sum_{m=1}^{M}|a_i||b_m|\cos\left(\frac{2\pi}{\lambda}\rho_i(\boldsymbol{v}_m)+\angle a_i b_m\right)\\
=&\sum_{i=1}^{L}|a_i|\sum_{m=1}^{M}|b_m|\cos\left(\bar{f}_i(\boldsymbol{v}_m)\right),
\end{aligned}\tag{57}$$

where $\bar{f}_i(\boldsymbol{v}_m)=\frac{2\pi}{\lambda}\rho_i(\boldsymbol{v}_m)+\angle(a_i b_m)$ and equation (f) holds for the same reason as equation (b) in (49). Based on the Taylor series expansion in (50), we have

$$\begin{aligned}
&\cos(\bar{f}_i(\boldsymbol{v}_m))\geq g(\bar{f}_i(\boldsymbol{v}_m)|\bar{f}_i(\boldsymbol{v}_{m,0}))\\
=&\cos\left(\bar{f}_i(\boldsymbol{v}_{m,0})\right)-\sin\left(\bar{f}_i(\boldsymbol{v}_{m,0})\right)\left(\bar{f}_i(\boldsymbol{v}_m)-\bar{f}_i(\boldsymbol{v}_{m,0})\right)\\
&-\frac{1}{2}\left(\bar{f}_i(\boldsymbol{v}_m)-\bar{f}_i(\boldsymbol{v}_{m,0})\right)^2\\
=&\cos\left(\bar{f}_i(\boldsymbol{v}_{m,0})\right)-\sin\left(\bar{f}_i(\boldsymbol{v}_{m,0})\right)\left(\frac{2\pi}{\lambda}[\rho_i(\boldsymbol{v}_m)-\rho_i(\boldsymbol{v}_{m,0})]\right)\\
&-\frac{1}{2}\left(\frac{2\pi}{\lambda}[\rho_i(\boldsymbol{v}_m)-\rho_i(\boldsymbol{v}_{m,0})]\right)^2\\
=&\frac{-2\pi^2}{\lambda^2}\left(\rho_i(\boldsymbol{v}_m)\right)^2+\frac{2\pi}{\lambda}\left[\frac{2\pi}{\lambda}\rho_i(\boldsymbol{v}_{m,0})-\sin\left(\bar{f}_i(\boldsymbol{v}_{m,0})\right)\right]\rho_i(\boldsymbol{v}_m)\\
&+\cos\left(\bar{f}_i(\boldsymbol{v}_{m,0})\right)+\frac{2\pi}{\lambda}\sin\left(\bar{f}_i(\boldsymbol{v}_{m,0})\right)\rho_i(\boldsymbol{v}_{m,0})-\frac{2\pi^2}{\lambda^2}\left(\rho_i(\boldsymbol{v}_{m,0})\right)^2,
\end{aligned}\tag{58}$$

which gives a lower-bound of (57) as

$$\begin{aligned}
\mathrm{Re}\{\boldsymbol{a}^T\boldsymbol{T}(\boldsymbol{V})^H\boldsymbol{b}\}\geq&\sum_{i=1}^{L}|a_i|\sum_{m=1}^{M}|b_m|g(\bar{f}_i(\boldsymbol{v}_m)|\bar{f}_i(\boldsymbol{v}_{m,0}))\\
=&\sum_{i=1}^{L}|a_i|(\boldsymbol{v}^T\tilde{\boldsymbol{\Lambda}}_i\boldsymbol{v}+\tilde{\boldsymbol{c}}_i\boldsymbol{v}+\tilde{d}_i)\\
=&\boldsymbol{v}^T\tilde{\boldsymbol{\Lambda}}\boldsymbol{v}+\tilde{\boldsymbol{c}}\boldsymbol{v}+\tilde{d},
\end{aligned}\tag{59}$$

where $\tilde{\boldsymbol{\Lambda}}=\sum_{i=1}^{L}|a_i|\tilde{\boldsymbol{\Lambda}}_i$, $\tilde{\boldsymbol{c}}=\sum_{i=1}^{L}|a_i|\tilde{\boldsymbol{c}}_i$, $\tilde{d}=\sum_{i=1}^{L}|a_i|\tilde{d}_i$,

$$\tilde{\boldsymbol{\Lambda}}_i=\frac{-2\pi^2}{\lambda^2}\begin{bmatrix}\tilde{\boldsymbol{A}}_i & \tilde{\boldsymbol{C}}_i\\ \tilde{\boldsymbol{C}}_i & \tilde{\boldsymbol{B}}_i\end{bmatrix},$$

$\tilde{\boldsymbol{A}}_i=\delta_i^2\mathrm{diag}(\bar{\boldsymbol{b}}),\tilde{\boldsymbol{B}}_i=\xi_i^2\mathrm{diag}(\bar{\boldsymbol{b}}),\tilde{\boldsymbol{C}}_i=\delta_i\xi_i\mathrm{diag}(\bar{\boldsymbol{b}})$,

$\tilde{\Upsilon}_m^i=\frac{2\pi}{\lambda}\rho_i(\boldsymbol{v}_{m,0})-\sin\left(\bar{f}_i(\boldsymbol{v}_{m,0})\right),\tilde{\boldsymbol{\Upsilon}}=[|b_1|\tilde{\Upsilon}_1^i,\ldots,|b_M|\tilde{\Upsilon}_M^i]$,

$$\tilde{\boldsymbol{c}}_i=\frac{2\pi}{\lambda}[\delta_i\tilde{\boldsymbol{\Upsilon}}_i,\xi_i\tilde{\boldsymbol{\Upsilon}}_i],\tilde{d}_i=\sum_{m=1}^{M}|b_m|\tilde{\varrho}_{i,m},$$

$$\tilde{\varrho}_{i,m}=\cos\left(\bar{f}_i(\boldsymbol{v}_{m,0})\right)+\frac{2\pi}{\lambda}\sin\left(\bar{f}_i(\boldsymbol{v}_{m,0})\right)\rho_i(\boldsymbol{v}_{m,0})-\frac{2\pi^2}{\lambda^2}\left(\rho_i(\boldsymbol{v}_{m,0})\right)^2,$$

and the definition of $\bar{\boldsymbol{b}}$ is given in (52). Since $\boldsymbol{v}^T\tilde{\boldsymbol{\Lambda}}_i\boldsymbol{v}=\frac{-2\pi^2}{\lambda^2}\sum_{m=1}^{M}|b_m|\left(\rho_i(\boldsymbol{v}_m)\right)^2\leq 0$, $\tilde{\boldsymbol{\Lambda}}_i$ is NSD. Therefore, $\tilde{\boldsymbol{\Lambda}}=\sum_{i=1}^{L}|a_i|\tilde{\boldsymbol{\Lambda}}_i$ is also NSD, which proves Theorem 2.

Appendix C
Proof of Theorem 3

For any vectors $\boldsymbol{a}=[a_1,\ldots,a_L]^T$, $\boldsymbol{b}=[b_1,\ldots,b_M]^T$, and $\check{\boldsymbol{a}}=[\check{a}_1,\ldots,\check{a}_{\check{L}}]^T$, we have $\boldsymbol{a}^T\boldsymbol{T}_\chi^H(\boldsymbol{V})\boldsymbol{b}=\sum_{i=1}^{L}\sum_{m=1}^{M}a_i(t_i^\chi(\boldsymbol{v}_m))^H b_m$ and $\check{\boldsymbol{a}}^T\boldsymbol{T}_{\check{\chi}}^H(\boldsymbol{V})\boldsymbol{b}=\sum_{l=1}^{\check{L}}\sum_{n=1}^{M}\check{a}_l(t_l^{\check{\chi}}(\boldsymbol{v}_n))^H b_n$, where $t_i^\chi(\boldsymbol{v}_m)=e^{-j\frac{2\pi}{\lambda}\rho_i^\chi(\boldsymbol{v}_m)}$ and $t_i^{\check{\chi}}(\boldsymbol{v}_m)=e^{-j\frac{2\pi}{\lambda}\rho_i^{\check{\chi}}(\boldsymbol{v}_m)}$. Then, it is known that

$$\begin{aligned}
&\mathrm{Re}\left\{\left(\boldsymbol{a}^T\boldsymbol{T}_\chi^H(\boldsymbol{V})\boldsymbol{b}\right)\left(\check{\boldsymbol{a}}^T\boldsymbol{T}_{\check{\chi}}^H(\boldsymbol{V})\boldsymbol{b}\right)^H\right\}\\
=&\mathrm{Re}\left\{\sum_{i=1}^{L}\sum_{m=1}^{M}\sum_{l=1}^{\check{L}}\sum_{n=1}^{M}a_i(t_i^\chi(\boldsymbol{v}_m))^H b_m b_n^H t_l^{\check{\chi}}(\boldsymbol{v}_n)\check{a}_l^H\right\}\\
=&\mathrm{Re}\left\{\sum_{i=1}^{L}\sum_{m=1}^{M}\sum_{l=1}^{\check{L}}\sum_{n=1}^{M}a_i b_m b_n^H\check{a}_l^H e^{j\frac{2\pi}{\lambda}[\rho_i^\chi(\boldsymbol{v}_m)-\rho_l^{\check{\chi}}(\boldsymbol{v}_n)]}\right\}\\
=&\sum_{i=1}^{L}\sum_{m=1}^{M}\sum_{l=1}^{\check{L}}\sum_{n=1}^{M}\mathrm{Re}\left\{a_i b_m b_n^H\check{a}_l^H e^{j\frac{2\pi}{\lambda}[\rho_i^\chi(\boldsymbol{v}_m)-\rho_l^{\check{\chi}}(\boldsymbol{v}_n)]}\right\}\\
=&\sum_{i=1}^{L}\sum_{m=1}^{M}\sum_{l=1}^{\check{L}}\sum_{n=1}^{M}|a_i b_m b_n\check{a}_l|\cos\left(\check{f}_{i,l}(\boldsymbol{v}_m,\boldsymbol{v}_n)\right)\\
\overset{\text{(g)}}{=}&\sum_{i=1}^{L}\sum_{m=1}^{M}\sum_{l=1}^{\check{L}}\sum_{n=1}^{M}|a_i||b_m||b_n||\check{a}_l|\cos\left(\check{f}_{i,l}(\boldsymbol{v}_m,\boldsymbol{v}_n)\right)\\
=&\sum_{i=1}^{L}\sum_{l=1}^{\check{L}}|a_i||\check{a}_l|\left[\sum_{m=1}^{M}\sum_{n=1}^{M}|b_m||b_n|\cos(\check{f}_{i,l}(\boldsymbol{v}_m,\boldsymbol{v}_n))\right],
\end{aligned}\tag{60}$$

where $\check{f}_{i,l}(\boldsymbol{v}_m,\boldsymbol{v}_n)=\frac{2\pi}{\lambda}[\rho_i^\chi(\boldsymbol{v}_m)-\rho_l^{\check{\chi}}(\boldsymbol{v}_n)]+\angle(a_i b_m b_n^H\check{a}_l^H)$, and equation (g) holds due to the same reason as equation (b) in (49). According to (54), we have

$$\begin{aligned}
&\cos(\check{f}_{i,l}(\boldsymbol{v}_m,\boldsymbol{v}_n))\leq\bar{g}(\check{f}_{i,l}(\boldsymbol{v}_m,\boldsymbol{v}_n)|\check{f}_{i,l}(\boldsymbol{v}_{m,0},\boldsymbol{v}_{n,0}))\\
=&\frac{2\pi^2}{\lambda^2}\left(\check{z}_{i,l}(\boldsymbol{v}_m,\boldsymbol{v}_n)\right)^2-\frac{2\pi}{\lambda}\left(\check{\tau}_{i,l,m,n}+\sin(\check{f}_{i,l,m,n}^0)\right)\check{z}_{i,l}(\boldsymbol{v}_m,\boldsymbol{v}_n)\\
&+\cos\left(\check{f}_{i,l,m,n}^0\right)+\sin\left(\check{f}_{i,l,m,n}^0\right)\check{\tau}_{i,l,m,n}+\frac{1}{2}\check{\tau}_{i,l,m,n}^2,
\end{aligned}\tag{61}$$

where $\check{f}_{i,l,m,n}^0=\check{f}_{i,l}(\boldsymbol{v}_{m,0},\boldsymbol{v}_{n,0})$, $\check{\tau}_{i,l,m,n}=\frac{2\pi}{\lambda}[\rho_i^\chi(\boldsymbol{v}_{m,0})-\rho_l^{\check{\chi}}(\boldsymbol{v}_{n,0})]$, and $\check{z}_{i,l}(\boldsymbol{v}_m,\boldsymbol{v}_n)=\rho_i^\chi(\boldsymbol{v}_m)-\rho_l^{\check{\chi}}(\boldsymbol{v}_n)=x_m^{\mathrm{t}}\delta_i^\chi+y_m^{\mathrm{t}}\xi_i^\chi-x_n^{\mathrm{t}}\delta_l^{\check{\chi}}-y_n^{\mathrm{t}}\xi_l^{\check{\chi}}$.

Although the expressions of (55) and (61) look similar, the construction of the convex surrogate function of $\mathrm{Re}\{\left(\boldsymbol{a}^T\boldsymbol{T}_\chi^H(\boldsymbol{V})\boldsymbol{b}\right)\left(\check{\boldsymbol{a}}^T\boldsymbol{T}_{\check{\chi}}^H(\boldsymbol{V})\boldsymbol{b}\right)^H\}$ is very different from that of $\mathrm{Re}\{\left(\boldsymbol{a}^T\boldsymbol{T}_\chi^H(\boldsymbol{V})\boldsymbol{b}\right)\}$, since the corresponding angles in $\rho_l^{\check{\chi}}(\boldsymbol{v}_n)$ are different from those in $\rho_l^\chi(\boldsymbol{v}_n)$.

Using (61), an upper-bound of (60) can be found as

$$\begin{aligned}
&\mathrm{Re}\left\{\left(\boldsymbol{a}^T\boldsymbol{T}_{\chi}^H(\boldsymbol{V})\boldsymbol{b}\right)\left(\check{\boldsymbol{a}}^T\boldsymbol{T}_{\check{\chi}}^H(\boldsymbol{V})\boldsymbol{b}\right)^H\right\}\\
\leq&\sum_{i=1}^{L}\sum_{l=1}^{\check{L}}|a_i||\check{a}_l|\left[\sum_{m=1}^{M}\sum_{n=1}^{M}|b_m||b_n|\bar{g}\left(\check{f}_{i,l}(\boldsymbol{v}_m,\boldsymbol{v}_n)|\check{f}_{i,l}(\boldsymbol{v}_{m,0},\boldsymbol{v}_{n,0})\right)\right]\\
=&\sum_{i=1}^{L}\sum_{l=1}^{\check{L}}|a_i||\check{a}_l|\left[\boldsymbol{v}^T\check{\boldsymbol{\Lambda}}_{i,l}\boldsymbol{v}+\check{\boldsymbol{c}}_{i,l}\boldsymbol{v}+\check{d}_{i,l}\right], \qquad (62)
\end{aligned}$$

where

$$\begin{aligned}
\check{\boldsymbol{\Lambda}}_{i,l}&=\frac{2\pi^2}{\lambda^2}\begin{bmatrix}\check{\boldsymbol{A}}_{i,l} & \check{\boldsymbol{C}}_{i,l}\\ \check{\boldsymbol{C}}_{i,l} & \check{\boldsymbol{B}}_{i,l}\end{bmatrix},\\
\check{\boldsymbol{A}}_{i,l}&=\left((\delta_i^{\chi})^2+(\delta_l^{\check{\chi}})^2\right)\mathrm{diag}(\kappa\bar{\boldsymbol{b}})-2\delta_i^{\chi}\delta_l^{\check{\chi}}\bar{\boldsymbol{b}}\bar{\boldsymbol{b}}^T,\\
\check{\boldsymbol{B}}_{i,l}&=\left((\xi_i^{\chi})^2+(\xi_l^{\check{\chi}})^2\right)\mathrm{diag}(\kappa\bar{\boldsymbol{b}})-2\xi_i^{\chi}\xi_l^{\check{\chi}}\bar{\boldsymbol{b}}\bar{\boldsymbol{b}}^T,\\
\check{\boldsymbol{C}}_{i,l}&=(\delta_i^{\chi}\xi_i^{\chi}+\delta_l^{\check{\chi}}\xi_l^{\check{\chi}})\mathrm{diag}(\kappa\bar{\boldsymbol{b}})-(\delta_i^{\chi}\xi_l^{\check{\chi}}+\delta_l^{\check{\chi}}\xi_i^{\chi})\bar{\boldsymbol{b}}\bar{\boldsymbol{b}}^T,\\
\check{\boldsymbol{c}}_{i,l}&=\frac{-2\pi}{\lambda}[\delta_i^{\chi}\check{\boldsymbol{\Upsilon}}_{i,l}-\delta_l^{\check{\chi}}\check{\boldsymbol{\Psi}}_{i,l},\xi_i^{\chi}\check{\boldsymbol{\Upsilon}}_{i,l}-\xi_l^{\check{\chi}}\check{\boldsymbol{\Psi}}_{i,l}]^T,\\
\check{\boldsymbol{\Upsilon}}_{i,l}&=[|b_1|\check{\Upsilon}_1^{i,l},\ldots,|b_M|\check{\Upsilon}_M^{i,l}]^T,\\
\check{\boldsymbol{\Psi}}_{i,l}&=[|b_1|\check{\Psi}_1^{i,l},\ldots,|b_M|\check{\Psi}_M^{i,l}]^T,\\
\check{\Upsilon}_m^{i,l}&=\sum_{n=1}^{M}|b_n|\left(\check{\tau}_{i,l,m,n}+\sin(\check{f}_{i,l,m,n}^0)\right),\\
\check{\Psi}_n^{i,l}&=\sum_{m=1}^{M}|b_m|\left(\check{\tau}_{i,l,m,n}+\sin(\check{f}_{i,l,m,n}^0)\right),\\
\check{d}_{i,l}&=\sum_{m=1}^{M}\sum_{n=1}^{M}|b_m||b_n|\check{\varrho}_{i,l,m,n},\\
\check{\varrho}_{i,l,m,n}&\triangleq\cos\left(\check{f}_{i,l,m,n}^0\right)+\sin\left(\check{f}_{i,l,m,n}^0\right)\check{\tau}_{i,l,m,n}+\frac{1}{2}\check{\tau}_{i,l,m,n}^2,
\end{aligned}$$

with κ and $\bar{\boldsymbol{b}}$ are given in (52).

Defining $\check{\boldsymbol{\Lambda}}=\sum_{i=1}^{L}\sum_{l=1}^{\check{L}}|a_i||\check{a}_l|\check{\boldsymbol{\Lambda}}_{i,l}$, $\check{\boldsymbol{c}}=\sum_{i=1}^{L}\sum_{l=1}^{\check{L}}|a_i||\check{a}_l|\check{\boldsymbol{c}}_{i,l}$, and $\check{d}=\sum_{i=1}^{L}\sum_{l=1}^{\check{L}}|a_i||\check{a}_l|\check{d}_{i,l}$, (62) can then be simplified as

$$\mathrm{Re}\left\{\left(\boldsymbol{a}^T\boldsymbol{T}_{\chi}^H(\boldsymbol{V})\boldsymbol{b}\right)\left(\check{\boldsymbol{a}}^T\boldsymbol{T}_{\check{\chi}}^H(\boldsymbol{V})\check{\boldsymbol{b}}\right)^H\right\}\leq\boldsymbol{v}^T\check{\boldsymbol{\Lambda}}\boldsymbol{v}+\check{\boldsymbol{c}}\boldsymbol{v}+\check{d}. \qquad (63)$$

Since $\check{\boldsymbol{\Lambda}}_{i,l}$ is in a symmetric form and $\boldsymbol{v}^T\check{\boldsymbol{\Lambda}}_{i,l}\boldsymbol{v}=\frac{2\pi^2}{\lambda^2}\sum_{m=1}^{M}\sum_{n=1}^{M}|b_m||b_n|\left(\check{z}_{i,l}(\boldsymbol{v}_m,\boldsymbol{v}_n)\right)^2\geq 0$, $\check{\boldsymbol{\Lambda}}_{i,l}$ is a PSD matrix, and so is $\check{\boldsymbol{\Lambda}}=\sum_{i=1}^{L}\sum_{l=1}^{\check{L}}|a_i||\check{a}_l|\check{\boldsymbol{\Lambda}}_{i,l}$. As a consequence, Theorem 3 is now proven.

Appendix D
Proof of Lemma 2

Subscript χ_2 is omitted here for brevity. For vectors $\boldsymbol{a}=[a_1,\ldots,a_L]^T$ and $\boldsymbol{b}=[b_1,\ldots,b_N]^T$, we know that

$$\begin{aligned}
\mathrm{Re}\left\{\boldsymbol{b}^T\boldsymbol{R}(\boldsymbol{U})\boldsymbol{a}\right\}&=\mathrm{Re}\left\{\sum_{i=1}^{L}\sum_{m=1}^{N}a_ir_i(\boldsymbol{u}_m)b_m\right\}\\
&=\mathrm{Re}\left\{\sum_{i=1}^{L}\sum_{m=1}^{N}a_ib_me^{-j\frac{2\pi}{\lambda}\rho_i(\boldsymbol{u}_m)}\right\}\\
&=\sum_{i=1}^{L}\sum_{m=1}^{N}|a_ib_m|\cos\left(-\frac{2\pi}{\lambda}\rho_i(\boldsymbol{u}_m)+\angle a_ib_m\right)\\
&\overset{\text{(h)}}{=}\sum_{i=1}^{L}\sum_{m=1}^{N}|a_i||b_m|\cos\left(-\frac{2\pi}{\lambda}\rho_i(\boldsymbol{u}_m)+\angle a_ib_m\right)\\
&=\sum_{i=1}^{L}|a_i|\sum_{m=1}^{N}|b_m|\cos\left(\bar{f}_i'(\boldsymbol{u}_m)\right), \qquad (64)
\end{aligned}$$

where $\bar{f}_i'(\boldsymbol{u}_m)=\frac{-2\pi}{\lambda}\rho_i(\boldsymbol{u}_m)+\angle(a_ib_m)$ and equation (h) holds for the same reason as equation (b) in (49).

Based on the Taylor series expansion in (50), a lower bound of (64) is written as

$$\begin{aligned}
&\cos(\bar{f}_i'(\boldsymbol{u}_m))\geq g(\bar{f}_i'(\boldsymbol{u}_m)|\bar{f}_i'(\boldsymbol{u}_{m,0}))\\
=&\cos\left(\bar{f}_i'(\boldsymbol{u}_{m,0})\right)-\sin\left(\bar{f}_i'(\boldsymbol{u}_{m,0})\right)\left(\bar{f}_i'(\boldsymbol{u}_m)-\bar{f}_i'(\boldsymbol{u}_{m,0})\right)\\
&-\frac{1}{2}\left(\bar{f}_i'(\boldsymbol{u}_m)-\bar{f}_i'(\boldsymbol{u}_{m,0})\right)^2\\
=&\cos\left(\bar{f}_i'(\boldsymbol{u}_{m,0})\right)+\sin\left(\bar{f}_i'(\boldsymbol{u}_{m,0})\right)\left(\frac{2\pi}{\lambda}[\rho_i(\boldsymbol{u}_m)-\rho_i(\boldsymbol{u}_{m,0})]\right)\\
&-\frac{1}{2}\left(\frac{2\pi}{\lambda}[\rho_i(\boldsymbol{u}_m)-\rho_i(\boldsymbol{u}_{m,0})]\right)^2\\
=&\frac{-2\pi^2}{\lambda^2}\left(\rho_i(\boldsymbol{u}_m)\right)^2+\frac{2\pi}{\lambda}\left[\frac{2\pi}{\lambda}\rho_i(\boldsymbol{u}_{m,0})+\sin\left(\bar{f}_i'(\boldsymbol{u}_{m,0})\right)\right]\rho_i(\boldsymbol{u}_m)\\
&+\cos\left(\bar{f}_i'(\boldsymbol{u}_{m,0})\right)-\frac{2\pi}{\lambda}\sin\left(\bar{f}_i'(\boldsymbol{u}_{m,0})\right)\rho_i(\boldsymbol{u}_{m,0})-\frac{2\pi^2}{\lambda^2}\left(\rho_i(\boldsymbol{u}_{m,0})\right)^2. \qquad (65)
\end{aligned}$$

Note that the Taylor series expansion of (64) is different from that of (57) due to the negative term in $\bar{f}_i'(\boldsymbol{u}_m)$. Thus, the concave quadratic surrogate function cannot be constructed directly from Theorem 2. A concave quadratic surrogate function of $\mathrm{Re}\{\boldsymbol{b}^T\boldsymbol{R}(\boldsymbol{U})\boldsymbol{a}\}$ can be obtainted using (65) as

$$\begin{aligned}
\mathrm{Re}\left\{\boldsymbol{b}^T\boldsymbol{R}(\boldsymbol{U})\boldsymbol{a}\right\}&\geq\sum_{i=1}^{L}|a_i|\sum_{m=1}^{N}|b_m|g(\bar{f}_i'(\boldsymbol{u}_m)|\bar{f}_i'(\boldsymbol{u}_{m,0}))\\
&=\sum_{i=1}^{L}|a_i|(\boldsymbol{u}^T\tilde{\boldsymbol{\Omega}}_i\boldsymbol{u}+\tilde{\boldsymbol{p}}_i\boldsymbol{u}+\tilde{q}_i)\\
&=\boldsymbol{u}^T\tilde{\boldsymbol{\Omega}}\boldsymbol{u}+\tilde{\boldsymbol{p}}\boldsymbol{u}+\tilde{q}, \qquad (66)
\end{aligned}$$

where $\tilde{\boldsymbol{\Omega}}=\sum_{i=1}^{L}|a_i|\tilde{\boldsymbol{\Omega}}_i$, $\tilde{\boldsymbol{p}}=\sum_{i=1}^{L}|a_i|\tilde{\boldsymbol{p}}_i$, $\tilde{q}=\sum_{i=1}^{L}|a_i|\tilde{q}_i$,

$$\tilde{\boldsymbol{\Omega}}_i=\frac{-2\pi^2}{\lambda^2}\begin{bmatrix}\tilde{\boldsymbol{A}}_i' & \tilde{\boldsymbol{C}}_i'\\ \tilde{\boldsymbol{C}}_i' & \tilde{\boldsymbol{B}}_i'\end{bmatrix},$$

$\tilde{\boldsymbol{A}}_i'=\delta_i^2\mathrm{diag}(\hat{\boldsymbol{b}}),\tilde{\boldsymbol{B}}_i'=\xi_i^2\mathrm{diag}(\hat{\boldsymbol{b}}),\tilde{\boldsymbol{C}}_i'=\delta_i\xi_i\mathrm{diag}(\hat{\boldsymbol{b}})$,

$\hat{\boldsymbol{b}}\triangleq[|b_1|,\ldots,|b_N|]^T$,

$$\tilde{\boldsymbol{p}}_i=\frac{2\pi}{\lambda}[\delta_i\tilde{\boldsymbol{\epsilon}}_i,\xi_i\tilde{\boldsymbol{\epsilon}}_i]^T,\tilde{q}_i=\sum_{m=1}^{M}|b_m|\tilde{\varrho}_{i,m}',$$

$$\tilde{\boldsymbol{\epsilon}}_i=[|b_1|\tilde{\epsilon}_1^i,\ldots,|b_N|\tilde{\epsilon}_N^i]^T,\tilde{\epsilon}_m^i=\frac{2\pi}{\lambda}\rho_i(\boldsymbol{u}_{m,0})+\sin\left(\bar{f}_i'(\boldsymbol{u}_{m,0})\right),$$

$$\tilde{\varrho}_{i,m}'=\cos\left(\bar{f}_i'(\boldsymbol{u}_{m,0})\right)-\frac{2\pi}{\lambda}\sin\left(\bar{f}_i'(\boldsymbol{u}_{m,0})\right)\rho_i(\boldsymbol{u}_{m,0})-\frac{2\pi^2}{\lambda^2}\left(\rho_i(\boldsymbol{u}_{m,0})\right)^2,$$

Since $\tilde{\boldsymbol{\Omega}}_i$ is symmetric and $\boldsymbol{u}^T\tilde{\boldsymbol{\Omega}}_i\boldsymbol{u}=\frac{-2\pi^2}{\lambda^2}\sum_{m=1}^{N}|b_m|\left(\rho_i(\boldsymbol{u}_m)\right)^2\leq 0$, $\tilde{\boldsymbol{\Omega}}_i$ is an NSD matrix, and so is $\tilde{\boldsymbol{\Omega}}$. Lemma 2 is thus proven.

REFERENCES

[1] Y. Zeng *et al.*, "A tutorial on environment-aware communications via channel knowledge map for 6G," *IEEE Commun. Surv. & Tuts.*, vol. 26, no. 3, pp. 1478–1519, 3rd Quart. 2024.

[2] M. Giordani, M. Polese, M. Mezzavilla, S. Rangan, and M. Zorzi, "Toward 6G networks: Use cases and technologies," *IEEE Commun. Mag.*, vol. 58, no. 3, pp. 55–61, Mar. 2020.

[3] F. Tariq *et al.*, "A speculative study on 6G," *IEEE Wireless Commun.*, vol. 27, no. 4, pp. 118–125, Aug. 2020.

[4] X. You *et al.*, "Toward 6G TKμ extreme connectivity: Architecture, key technologies and experiments," *IEEE Wireless Commun.*, vol. 30, no. 3, pp. 86–95, Jun. 2023.

[5] D. A. Urquiza Villalonga, H. OdetAlla, M. J. Fernández-Getino Garcia, and A. Flizikowski, "Spectral efficiency of precoded 5G-NR in single and multi-user scenarios under imperfect channel knowledge: A comprehensive guide for implementation," *Electronics*, vol. 11, no. 24 (article number: 4237), Dec. 2022.

[6] K.-K. Wong, R. D. Murch, R.-K. Cheng, and K. B. Letaief, "Optimizing the spectral efficiency of multiuser MIMO smart antenna systems," in *Proc. IEEE Wireless Commun. Netw. Conf.*, vol. 1, pp. 426–430, 23-28 Sept. 2000, Chicago, IL, USA.

[7] K.-K. Wong, R. D. Murch and K. B. Letaief, "Performance enhancement of multiuser MIMO wireless communication systems," *IEEE Trans. Commun.*, vol. 50, no. 12, pp. 1960–1970, Dec. 2002.

[8] S. Vishwanath, N. Jindal and A. Goldsmith, "Duality, achievable rates, and sum-rate capacity of Gaussian MIMO broadcast channels," *IEEE Trans. Inf. Theory*, vol. 49, no. 10, pp. 2658–2668, Oct. 2003.

[9] Q. H. Spencer, A. L. Swindlehurst and M. Haardt, "Zero-forcing methods for downlink spatial multiplexing in multiuser MIMO channels," *IEEE Trans. Sig. Process.*, vol. 52, no. 2, pp. 461–471, Feb. 2004.

[10] T. L. Marzetta, "Noncooperative cellular wireless with unlimited numbers of base station antennas," *IEEE Trans. Wireless Commun.*, vol. 9, no. 11, pp. 3590–3600, Nov. 2010.

[11] E. G. Larsson, O. Edfors, F. Tufvesson and T. L. Marzetta, "Massive MIMO for next generation wireless systems," *IEEE Commun. Mag.*, vol. 52, no. 2, pp. 186–195, Feb. 2014.

[12] Z. Wang *et al.*, "A tutorial on extremely large-scale MIMO for 6G: Fundamentals, signal processing, and applications," *IEEE Commun. Surv. & Tut.*, vol. 26, no. 3, pp. 1560–1605, thirdquarter 2024.

[13] K.-K. Wong, K.-F. Tong, Y. Zhang, and Z. Zheng, "Fluid antenna system for 6G: When Bruce Lee inspires wireless communications," *Elect. Lett.*, vol. 56, no. 24, pp. 1288–1290, Nov. 2020.

[14] K. K. Wong, A. Shojaeifard, K.-F. Tong, and Y. Zhang, "Performance limits of fluid antenna systems," *IEEE Commun. Lett.*, vol. 24, no. 11, pp. 2469–2472, Nov. 2020.

[15] K.-K. Wong, A. Shojaeifard, K.-F. Tong, and Y. Zhang, "Fluid antenna systems," *IEEE Trans. Wireless Commun.*, vol. 20, no. 3, pp. 1950–1962, Mar. 2021.

[16] W. K. New *et al.*, "A tutorial on fluid antenna system for 6G networks: Encompassing communication theory, optimization methods and hardware designs," *IEEE Commun. Surv. & Tuts.*, doi:10.1109/COMST.2024.3498855, 2024.

[17] W.-J. Lu *et al.*, "Fluid antennas: Reshaping intrinsic properties for flexible radiation characteristics in intelligent wireless networks," *IEEE Commun. Mag.*, vol. 63, no. 5, pp. 40–45, May 2025.

[18] Y. Huang, L. Xing, C. Song, S. Wang, and F. Elhouni, "Liquid antennas: Past, present and future," *IEEE Open J. Antennas Propag.*, vol. 2, pp. 473–487, Mar. 2021.

[19] Y. Shen *et al.*, "Design and implementation of mmWave surface wave enabled fluid antennas and experimental results for fluid antenna multiple access," *arXiv preprint*, arXiv:2405.09663, May 2024.

[20] S. Basbug, "Design and synthesis of antenna array with movable elements along semicircular paths," *IEEE Antennas Wireless Propag. Lett.*, vol. 16, pp. 3059–3062, Oct. 2017.

[21] L. Zhu and K.-K. Wong, "Historical review of fluid antenna and movable antenna," *arXiv preprint*, arXiv:2401.02362v2, 2024.

[22] T. V. Hoang, V. Fusco, T. Fromenteze and O. Yurduseven, "Computational polarimetric imaging using two-dimensional dynamic metasurface apertures," *IEEE Open J. Antennas & Propag.*, vol. 2, pp. 488–497, Mar. 2021.

[23] M. C. Johnson, S. L. Brunton, N. B. Kundtz, and J. N. Kutz, "Sidelobe canceling for reconfigurable holographic metamaterial antenna," *IEEE Trans. Antennas Propag.*, vol. 63, no. 4, pp. 1881–1886, Apr. 2015.

[24] B. Liu, K. F. Tong, K. K. Wong, C.-B. Chae, and H. Wong, "Be water, my antennas: Riding on radio wave fluctuation in nature for spatial multiplexing using programmable meta-fluid antenna," *arXiv preprint*, arXiv:2502.04693, 2025.

[25] L. Jing, M. Li, and R. Murch, "Compact pattern reconfigurable pixel antenna with diagonal pixel connections," *IEEE Trans. Antennas Propag.*, vol. 70, no. 10, pp. 8951–8961, Oct. 2022.

[26] J. Zhang *et al.*, "A novel pixel-based reconfigurable antenna applied in fluid antenna systems with high switching speed," *IEEE Open J. Antennas Propag.*, vol. 6, no. 1, pp. 212–228, Feb. 2025.

[27] L. Tlebaldiyeva, S. Arzykulov, A. Dadlani, K. M. Rabie, and G. Nauryzbayev, "Exploring the performance of fluid antenna system (FAS)-aided B5G mmWave networks," in *Proc. IEEE Global Commun. Conf. (Globecom)*, pp. 7568–7573, 4-8 Dec. 2023, Kuala Lumpur, Malaysia.

[28] M. Khammassi, A. Kammoun and M.-S. Alouini, "A new analytical approximation of the fluid antenna system channel," *IEEE Trans. Wireless Commun.*, vol. 22, no. 12, pp. 8843–8858, Dec. 2023.

[29] J. D. Vega-Sánchez, L. Urquiza-Aguiar, M. C. P. Paredes, and D. P. M. Osorio, "A simple method for the performance analysis of fluid antenna systems under correlated Nakagami-m fading," *IEEE Wireless Commun. Lett.*, vol. 13, no. 2, pp. 377–381, Feb. 2024.

[30] P. D. Alvim *et al.*, "On the performance of fluid antennas systems under α-μ fading channels," *IEEE Wireless Commun. Lett.*, vol. 13, no. 1, pp. 108–112, Jan. 2024.

[31] W. K. New, K. K. Wong, H. Xu, K. F. Tong and C. B. Chae, "Fluid antenna system: New insights on outage probability and diversity gain," *IEEE Trans. Wireless Commun.*, vol. 23, no. 1, pp. 128–140, Jan. 2024.

[32] C. Psomas, P. J. Smith, H. A. Suraweera, and I. Krikidis, "Continuous fluid antenna systems: Modeling and analysis," *IEEE Commun. Lett.*, vol. 27, no. 12, pp. 3370–3374, Dec. 2023.

[33] W. K. New, K. K. Wong, H. Xu, K. F. Tong, and C.-B. Chae, "An information-theoretic characterization of MIMO-FAS: Optimization, diversity-multiplexing tradeoff and q-outage capacity," *IEEE Trans. Wireless Commun.*, vol. 23, no. 6, pp. 5541–5556, Jun. 2024.

[34] H. Xu *et al.*, "Capacity maximization for FAS-assisted multiple access channels," *IEEE Trans. Commun.*, vol. 73, no. 7, pp. 4713–4731, Jul. 2025.

[35] M. Olyaee and S. Buzzi, "User-centric cell-free massive MIMO with access points empowered by fluid antennas," in *Proc. IEEE Int. Workshop Sig. Process. Adv. Wireless Commun. (SPAWC)*, pp. 666–670, 10-13 Sept. 2024, Lucca, Italy.

[36] K.-K. Wong and K.-F. Tong, "Fluid antenna multiple access," *IEEE Trans. Wireless Commun.*, vol. 21, no. 7, pp. 4801–4815, Jul. 2022.

[37] K. K. Wong, D. Morales-Jimenez, K. F. Tong, and C. B. Chae, "Slow fluid antenna multiple access," *IEEE Trans. Commun.*, vol. 71, no. 5, pp. 2831–2846, May 2023.

[38] H. Xu *et al.*, "Revisiting outage probability analysis for two-user fluid antenna multiple access system," *IEEE Trans. Wireless Commun.*, vol. 23, no. 8, pp. 9534–9548, Aug. 2024.

[39] Y. Chen, S. Li, Y. Hou, and X. Tao, "Energy-efficiency optimization for slow fluid antenna multiple access using mean-field game," *IEEE Wireless Commun. Lett.*, vol. 13, no. 4, pp. 915–918, Apr. 2024.

[40] K.-K. Wong, C.-B. Chae, and K.-F. Tong, "Compact ultra massive antenna array: A simple open-loop massive connectivity scheme," *IEEE Trans. Wireless Commun.*, vol. 23, no. 6, pp. 6279–6294, Jun. 2024.

[41] K.-K. Wong, "Transmitter CSI-free RIS-randomized CUMA for extreme massive connectivity," *IEEE Open J. Commun. Soc.*, vol. 5, pp. 6890–6902, Oct. 2024.

[42] H. Hong, K. K. Wong, K. F. Tong, H. Shin, and Y. Zhang, "Coded fluid antenna multiple access over fast fading channels," *IEEE Wireless Commun. Lett.*, vol. 14, no. 4, pp. 1249–1253, Apr. 2025.

[43] X. Lai *et al.*, "FAS-assisted wireless powered communication systems," in *IEEE Int. Conf. Commun. Workshops (ICC Workshops)*, pp. 1731–1736, 9-13 Jun. 2024, Denver, CO, USA.

[44] L. Zhou *et al.*, "Fluid antenna-assisted simultaneous wireless information and power transfer systems," *IEEE Trans. Veh. Technol.*, vol. 74, no. 5, pp. 8285–8290, May 2025.

[45] B. Tang *et al.*, "Fluid antenna enabling secret communications," *IEEE Commun. Lett.*, vol. 27, no. 6, pp. 1491–1495, Jun. 2023.

[46] F. R. Ghadi *et al.*, "Physical layer security over fluid antenna systems: Secrecy performance analysis," *IEEE Trans. Wireless Commun.*, vol. 23, no. 12, pp. 18201–18213, Dec. 2024.

[47] Y. Chen *et al.*, "Joint beamforming and antenna design for near-field fluid antenna system," *IEEE Wireless Commun. Lett.*, vol. 14, no. 2, pp. 415–419, Feb. 2025.

[48] Z. Zhang, J. Zhu, L. Dai, and R. W. Heath, "Successive bayesian reconstructor for channel estimation in fluid antenna systems," *IEEE Trans. Wireless Commun.*, vol. 24, no. 3, pp. 1992–2006, Mar. 2025.

[49] H. Xu *et al.*, "Channel estimation for FAS-assisted multiuser mmWave systems," *IEEE Commun. Lett.*, vol. 28, no. 3, pp. 632–636, Mar. 2024.

[50] C. Skouroumounis and I. Krikidis, "Fluid antenna with linear MMSE channel estimation for large-scale cellular networks," *IEEE Trans. Commun.*, vol. 71, no. 2, pp. 1112–1125, Feb. 2023.

[51] W. K. New *et al.*, "Channel estimation and reconstruction in fluid antenna system: Oversampling is essential," *IEEE Trans. Wireless Commun.*, vol. 24, no. 1, pp. 309–322, Jan. 2025.

[52] F. Liu *et al.*, "Integrated sensing and communications: Toward dual-functional wireless networks for 6G and beyond," *IEEE J. Sel. Areas Commun.*, vol. 40, no. 6, pp. 1728–1767, Jun. 2022.

[53] F. Liu, C. Masouros, A. P. Petropulu, H. Griffiths, and L. Hanzo, "Joint radar and communication design: Applications, state-of-the-art, and the road ahead," *IEEE Trans. Commun.*, vol. 68, no. 6, pp. 3834–3862, Jun. 2020.

[54] K. Meng, C. Masouros, A. P. Petropulu, and L. Hanzo, "Cooperative ISAC networks: Opportunities and challenges," *IEEE Wireless Commun.*, vol. 32, no. 3, pp. 212–219, Jun. 2025.

[55] C. Wang *et al.*, "Fluid antenna system liberating multiuser MIMO for ISAC via deep reinforcement learning," *IEEE Trans. Wireless Commun.*, vol. 23, no. 9, pp. 10 879–10 894, Sep. 2024.

[56] L. Zhou, J. Yao, M. Jin, T. Wu and K. K. Wong, "Fluid antenna-assisted ISAC systems," *IEEE Wireless Commun. Lett.*, vol. 13, no. 12, pp. 3533–3537, Dec. 2024.

[57] J. Zou *et al.*, "Shifting the ISAC trade-off with fluid antenna systems," *IEEE Wireless Commun. Lett.*, vol. 13, no. 12, pp. 3479–3483, Dec. 2024.

[58] W. Lyu *et al.*, "Movable antenna enabled integrated sensing and communication," *IEEE Trans. Wireless Commun.*, vol. 24, no. 4, pp. 2862–2875, Apr. 2025.

[59] C. Jiang *et al.*, "Movable antenna-assisted integrated sensing and communication systems," *IEEE Trans. Wireless Commun.*, doi:10.1109/TWC.2025.3552843, 2025.

[60] F. R. Ghadi, K.-K. Wong, F. J. Lopez-Martinez, H. Shin, and L. Hanzo, "Performance analysis of FAS-aided NOMA-ISAC: A backscattering scenario," *arXiv preprint*, arXiv:2408.04724, 2024.

[61] K. Meng, C. Masouros, K.-K. Wong, A. P. Petropulu, and L. Hanzo, "Integrated sensing and communication meets smart propagation engineering: Opportunities and challenges," *IEEE Netw.*, vol. 39, no. 2, pp. 278–285, Mar. 2025.

[62] Y. Liu *et al.*, "A full-duplex transceiver with two-stage analog cancellations for multipath self-interference," *IEEE Trans. Microw. Theory Tech.*, vol. 65, no. 12, pp. 5263–5273, Dec. 2017.

[63] C. Skouroumounis and I. Krikidis, "Fluid antenna-aided full duplex communications: A macroscopic point-of-view," *IEEE J. Sel. Areas Commun.*, vol. 41, no. 9, pp. 2879–2892, Sep. 2023.

[64] H. Hong *et al.*, "Fluid antenna system-assisted self-interference cancellation for in-band full duplex communications," *arXiv preprint*, arXiv:2506.05569, 2025.

[65] L. Tlebaldiyeva, S. Arzykulov, T. A. Tsiftsis and G. Nauryzbayev, "Full-duplex cooperative NOMA-based mmWave networks with fluid antenna system (FAS) receivers," in *Proc. Int. Balkan Conf. Commun. Netw. (BalkanCom)*, 5-8 Jun. 2023, Istanbul, Turkey.

[66] A. Tang, X. Wang and J. A. Zhang, "Interference management for full-duplex ISAC in B5G/6G networks: Architectures, challenges, and solutions," *IEEE Commun. Mag.*, vol. 62, no. 9, pp. 20–26, Sep. 2024.

[67] M. Ashraf, B. Tan, D. Moltchanov, J. S. Thompson, and M. Valkama, "Joint optimization of radar and communications performance in 6G cellular systems," *IEEE Trans. Green Commun. Netw.*, vol. 7, no. 1, pp. 522–536, Mar. 2023.

[68] K. Shen and W. Yu, "Fractional programming for communication systems–part I: Power control and beamforming," *IEEE Trans. Signal Process.*, vol. 66, no. 10, pp. 2616–2630, May 2018.

[69] ——, "Fractional programming for communication systems–part II: Uplink scheduling via matching," *IEEE Trans. Signal Process.*, vol. 66, no. 10, pp. 2631–2644, May 2018.